Faculty of Engineering of the University of Porto

Development of a Novel Hydrogel Dressing for Radiodermatitis Treatment

Céline Daniela Santos Costa

july 2022

Faculty of Engineering of the University of Porto

Development of a Novel Hydrogel Dressing for Radiodermatitis Treatment

Céline Daniela Santos Costa

Dissertation for the master in Biomedical Engineering

Supervisor: Dr. Joana Barros

Co-supervisors: Prof. Dr. Fernando Jorge Monteiro
Prof. Dr. Isabel Bravo

july 2022

Abstract

Every year, millions of people are diagnosed with cancer worldwide and radiotherapy plays an important role in their treatment. However, it can also cause uncomfortable or even painful side effects on the skin. The most common side effect of radiotherapy is radiodermatitis. These skin lesions could affect the success of the treatment and the quality of patient life. One therapeutic approach of relevance to skin wound healing is tissue engineering, in which the combination of a biomaterial, cells, and biological signals plays a decisive role in the regeneration of the damaged tissue. Hydrogels are considered suitable and ideal biomaterials for tissue engineering, due to their structural similarity to the skin extracellular matrix. Hydrogel-based dressings act as a three-dimensional scaffold, which can absorb the exuding liquids and debris from the wound area, maintaining a physiologically moist microenvironment and promoting wound healing. Alginate is one of the most common biopolymers used in wound healing and collagen is the most abundant protein in the human body. The combination of these two components in wound hydrogel-based dressings can provide a proper environment for the healing process.

At present work, a hydrogel-based dressing for radiodermatitis treatment was designed. The hydrogels were synthesized, and fully characterized in terms of morphology, chemical composition, swelling behavior, water content, pH-responsive behavior, and protein adsorption. Additionally, human dermal fibroblasts under and without radiation treatment were cultured to assess the *in vitro* cytocompatibility and regenerative effect of the hydrogels. The hydrogels were composed of alginate and type I collagen, in order to restore skin tissue integrity and hemostasis and decrease the side effects of radiotherapy. Morphologically, the hydrogels showed that temperature (37 ºC), incubation time (12 and 24 h) and collagen concentration (0.25 %) appear to induce an increase of collagen fibrils formation which could be important in promote cell adhesion and proliferation. From chemical analysis, it is possible to conclude that collagen can be incorporated into the alginate network without altering its chemical structure, even using different conditions of hydrogel production. Regarding the swelling behavior and water content, hydrogels showed a great ability to absorb exudate maintaining a physiologically moist environment. Additionally, they showed to be stable at different pH values (5.5, 7.4, and 8.0) and capable to adsorb proteins while maintaining their integrity. Furthermore, even after irradiation, the alginate-collagen hydrogels permitted human dermal fibroblasts to grow and proliferate with similar cell morphology and organization compared to control (without hydrogel), highlighting hydrogels biocompatibility. In sum, the developed hydrogel based on alginate and collagen showed promising properties in terms of maintaining a healthy physiological milieu and promoting cell proliferation even after radiotherapy.

Resumo

Todos os anos, milhões de pessoas são diagnosticadas com cancro em todo o mundo e a radioterapia desempenha um papel importante no seu tratamento. No entanto, também pode causar efeitos adversos desconfortáveis ou até dolorosos na pele. O efeito adverso mais comum da radioterapia é a radiodermite. Essas lesões cutâneas podem afetar o sucesso do tratamento e a qualidade de vida do doente. Uma abordagem terapêutica de relevância para a cicatrização de feridas cutâneas é a engenharia de tecidos, na qual a combinação de um biomaterial, células e sinais biológicos desempenha um papel decisivo na regeneração do tecido lesado. Os hidrogéis são considerados biomateriais adequados e ideais para a engenharia de tecidos, devido à sua semelhança estrutural com a matriz extracelular da pele. Os pensos à base de hidrogel atuam como uma matriz tridimensional, que pode absorver os exsudados e detritos da área afetada, mantendo um microambiente fisiologicamente húmido e promovendo a cicatrização da ferida. O alginato é um dos biopolímeros mais usados na cicatrização de feridas e o colagénio é a proteína mais abundante no corpo humano. A combinação desses dois componentes em pensos à base de hidrogel pode proporcionar um ambiente adequado para o processo de cicatrização.

No presente trabalho, foi desenvolvido um penso à base de hidrogel para tratamento de radiodermatites. Os hidrogéis foram sintetizados e totalmente caracterizados quanto à morfologia, composição química, capacidade de absorção e retenção de líquidos, resposta ao pH e adsorção de proteínas. Adicionalmente, fibroblastos da derme humana sob e sem tratamento com radiação foram cultivados para avaliar a citocompatibilidade *in vitro* e o efeito regenerativo dos hidrogéis. Os hidrogéis foram constituídos por alginato e colagénio tipo I, com o objetivo de restaurar a integridade e hemostasia da pele e diminuir os efeitos adversos da radioterapia. Morfologicamente, os hidrogéis mostraram que a temperatura (37 °C), o tempo de incubação (12 e 24 h) e a concentração de colagénio (0,25 %) parecem levar a um aumento na formação de fibrilas de colagénio que podem ser importantes em promover a adesão e proliferação celulares. A partir da análise química, é possível concluir que o colagénio pode ser incorporado na rede de alginato sem alterar a sua estrutura química, mesmo utilizando diferentes condições na síntese do hidrogel. Em relação à capacidade de absorção e retenção de líquidos, os hidrogéis mostraram uma grande capacidade para absorver exsudato mantendo um ambiente fisiologicamente húmido. Adicionalmente, mostraram-se estáveis em diferentes valores de pH (5,5, 7,4, e 8,0) e capazes de adsorver proteínas mantendo a sua integridade. Além disso, mesmo após a irradiação, os hidrogéis de alginato e colagénio permitiram que fibroblastos da derme humana crescessem e proliferassem com morfologia

e organização celular semelhante ao controlo (sem hidrogel), destacando a biocompatibilidade dos hidrogéis. Em suma, o hidrogel desenvolvido à base de alginato e colagénio mostrou propriedades promissoras em termos de manutenção de um meio fisiológico saudável e promoção da proliferação celular mesmo após radioterapia.

Acknowledgements

This dissertation would not have been possible without the support of many people.

I would first like to thank my supervisor, Dr. Joana Barros for giving me the opportunity to work on this project and for sharing knowledge and experience. Her guidance, encouragement, and enthusiasm instilled confidence in me, allowing me to focus on my studies in a productive and pleasurable manner. Thank you so much for welcoming me and for including me in the team.

I would also like to thank my co-supervisor, Prof. Dr. Fernando Jorge Monteiro for your support and precious suggestions.

Many thanks to my co-supervisor Prof. Dr Isabel Bravo, for the enthusiasm and support.

I wanted to acknowledge my colleagues from Biocomposites Group at Instituto de Investigação e Inovação em Saúde da Universidade do Porto, for their precious collaboration and support in the lab, for wise counsel, and for providing discussions as well as happy distractions. I would also like to thank Rui Rocha, Ana Rita Malheiro and Rossana Correia, for technical support in the SEM, TEM, and histological analysis, respectively. Many thanks to Ricardo Vidal, Liliana Grenho and Joana Lencart for your support in FTIR spectroscopy, cell culture, irradiation process, respectively.

Now, to my parents, thank you for always being there for me. I am so grateful for my family's unconditional, unequivocal, and loving support.

To my partner Hatus Deolindo, thank you for constantly listening to me, for motivating me every day even after difficult days at work or in the lab, for smiling and cracking jokes, and for the sacrifices you have made for me to pursue this master's degree.

To all my friends, a big thank you for dealing with me every day.

Contents

Figure List

Table list

Abbreviations and Acronyms

3D	Three-dimensional
Al^{3+}	Aluminium Ions
Alg	Alginate
ATR-FTIR	Attenuated Total Reflection - Fourier Transform Infrared
BSA	Bovine Serum Albumin
Ca^{2+}	Calcium Ions
$CaCl_2$	Calcium Chloride
Col	Collagen
ColI	Type I Collagen
CONH	Amide Group
COO	Carboxylic Group
COOH	Carboxyl Group
DMSO	Dimethyl Sulfoxide
DNA	Deoxyribonucleic Acid
ECM	Extracellular Matrix
FBS	Fetal Bovine Serum
Fe^{3+}	Iron Ions
Gy	Gray
HDF	Human Dermal Fibroblasts
NH2	Amino Group
OH	Hydroxyl Group
PBS	Phosphate-buffered Saline
RD	Radiodermatitis
RGD	Tripeptide Arginine-Glycine-Aspartate
RT	Room Temperature
RPM	Rotations Per Minute
RTOG	Radiation Therapy Oncology Group
SD	Standard Deviation
SEM	Scanning Electron Microscopy
SI	International System
TE	Tissue Engineering

TEM	Transmission Electron Microscopy
WHO	World Health Organization
α-MEM	Alpha-Minimum Essential Medium

Chapter 1

Introdution

In the current years, cancer is one of the most problematic medical conditions worldwide, and radiotherapy is a fundamental component of cancer treatment. Radiotherapy uses high doses of ionizing radiation to destroy cancer cells. However, the development of radiodermatitis, which is a skin lesion caused by radiation, is a significant adverse effect of this therapeutic modality.

In this chapter, radiotherapy, and its most common side effect – radiodermatitis – will be explained, and a solution, with the potential to replace and/or accelerate the reconstitution of damaged skin, will be explored.

1.1 - Radiotherapy

Cancer is a disease characterized by the uncontrolled growth of abnormal cells that can eventually spread to other parts of the body. In the current years, cancer is one of the most severe medical conditions and, according to the World Health Organization (WHO), is the second leading cause of death worldwide [1]. There are several therapeutic modalities available to treat cancer, but surgery, chemotherapy, and radiotherapy are the most commonly used. Approximately, 50 % of all cancer patients require radiotherapy during their course of illness [2].

Radiotherapy also called radiation therapy is a treatment that uses high doses of radiation to destroy cancer [2]. The distribution of radiation dose over time, known as fractionation, is one of the most important factors determining the outcome of radiotherapy. In general, the total radiation dose is divided into daily doses (range from 1,8 to 2 Gray), five days a week, for five to eight weeks. Gray (Gy) is the international system (SI) unit of absorbed dose, defined as 1 J/kg [3].

The radiation used in radiotherapy is called ionizing radiation because it forms ions as it passes through biological targets, causing damage. This radiation damage can be originated from two mechanisms, direct and indirect [4]. In the direct action of radiation, all atoms or molecules that are inside the cells are exposed to radiation injury. However, is the deoxyribonucleic acid (DNA) the vital target, in which ionizing radiation produces single or double-stranded chromosomal breaks. Instead, in the indirect mechanism, ionizing radiation exerts its biological effect via radiolysis of intracellular water, forming free radicals. These free radicals

interact with DNA, creating some physico-chemical modifications that can cause harmful effects [4, 5].

The biological effects of ionizing radiation can be influenced by factors related to the radiation itself and the target tissue. Type of radiation (e.g., photons or electrons) and fractionation (e.g., total dose and dose per fraction) are some of the factors related to radiation. In fact, various types of radiation differ in penetrability, and this can cause more or less damage. Also, the mode of administration of the radiation is an important factor, since a single dose causes more damage than the same dose being fractionated. In general, the total dose of radiotherapy is divided into daily doses to allow cellular repair of the healthy tissues. Importantly, the tissue damage builds up with every single delivery of radiation – the cumulative effect of radiation – and this is shown by the fact that, at the end of the radiotherapy treatment, patients developed some lesions that are non-existent at the beginning [4, 5]. Regarding the factors related to a biological target, it can be highlighted: (1) the tissue radiosensitivity, which varies with the rate of mitosis and cellular maturity, (2) the repair capacity of cells, where the effect of the same radiation dose is different in cells with higher capacity than other to repair radiation damages, (3) the cell-cycle phase (e.g., the post-DNA synthetic phase – G2 – and the mitosis phase – M – are the most sensitive to radiation) and (4) the degree of tissue oxygenation, since the presence of oxygen is known to have the ability to potentiate the response to radiation [6]. Therefore, actively proliferating cells (e.g., basal cells of the epidermis, which is a layer of the skin) are highly radiosensitive, i.e., sensitive to radiation [4]. Although radiotherapy is aimed at cancer, in most cases it affects the surrounding healthy tissue, such as the skin. Due to the skin radiosensitivity, radiotherapy can cause cutaneous lesions known as radiodermatitis [6].

Despite all advances in technology and improvement in treatment regimens, radiodermatitis remains a significant adverse effect of radiotherapy, and its prevention and management are still a challenge [6, 7].

1.2 – Radiodermititis

Radiodermatitis (RD) is a skin lesion that occurs as a side effect of radiotherapy treatment [5]. Approximately, 95 % of patients who receive radiotherapy will develop some form of RD during or after the course of treatment [6-8].

In healthy skin, there is a balance between cell growth and death of each cell type, while in RD the basal layer, which is an actively dividing layer of skin, is destroyed. Therefore, RD affects the balance between normal cell production in the basal layer and cell destruction on the skin surface. During radiotherapy treatments, radiation accumulates in the skin, altering its integrity and the healing process. This leads to structural, histologic, and vasculature changes of the skin [9].

The development of these lesions depends on several factors, including the type of radiation, fractionation, area of treatment, co-existing skin conditions and patient lifestyle [6-10].

The clinical manifestations of RD can be divided into: early/acute reactions and late/chronic reactions. These two forms of RD depend on the time the skin reaction occurs. Acute skin reactions develop a few hours to weeks after the first exposure to ionizing radiation, while chronic RD can occur months, years or even decades after radiotherapy. Both acute and chronic RD can impair the cosmetic outcome of the treatment and consequently the quality of life of patients [5].

Symptoms of acute and chronic RD can be graded on a scale of 1–4 according to the National Cancer Institute and the criteria of the Radiation Therapy Oncology Group (RTOG) as shown in Table 1.1 [5,11]. Acute RD (see Fig. 1.1) starts with skin rash, mild erythema, skin dryness and dry desquamation (grade 1). With higher doses of radiation, can occurs bright erythema combined with patchy moist desquamation (grade 2). When RD worsens, moist desquamation develops (grade 3). In some rare cases, necrosis with haemorrhage and eventually ulceration can occur (grade 4) [5, 6, 11].

Figure 1.1 – Acute radiodermatitis from (a) erythema to (b) dry and (c) moist desquamation. Adapted from [12].

Chronic RD is usually characterized by skin atrophy, fibrosis, pigmentation changes, telangiectasia, ulceration, and necrosis (see Table 1.1 and Fig. 1.2) [5].

RD can cause a lot of pain and, sometimes a premature interruption of radiotherapy is necessary, which will eventually affect the treatment outcome and, consequently, the overall survival rate. For that reason, it is very important to delineate a proper strategy for the prevention and treatment of acute RD [5, 6].

Nowadays, the prevention and treatment of RD still remain a challenge because, despite advancements in science and technology, and the development of new therapeutic options, there is no definitive evidence supporting any one intervention in the prevention or management of RD [7, 8]. As a result, each department of radiotherapy uses a different approach to prevent and manage acute RD [5]. Up to now, the therapeutic options of RD include emollient creams, topical corticosteroids, drying lotions and absorbent dressings [9]. Therefore, it is necessary to perform more studies to reach a universal consensus.

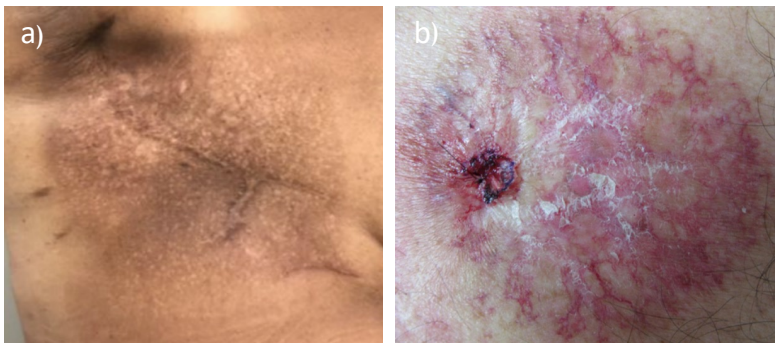

Figure 1.2 – Chronic radiodermatitis from (a) pigmentation change to (b) telangiectasia and ulceration. Adapted from [6, 13].

Table 1.1 — Radiation Therapy Oncology Group radiation morbidity scoring for radiotherapy-induced skin injuries.

	RTOG Grade				
Onset	**0**	**1**	**2**	**3**	**4**
Acute	No change over baseline	Follicular, faint or dull erythema; epilation; possible dry desquamation; decreased sweating	Tender or bright erythema; patchy moist desquamation; moderate edema	Confluent, moist desquamation other than skin folds; pitting edema	Ulceration; hemorrhage; necrosis
Chronic	None	Slight atrophy; pigmentation change; some hair loss	Patchy atrophy; moderate telangiectasia; total hair loss	Marked atrophy; gross telangiectasia	Ulceration; necrosis

1.3 – Skin

The skin is the largest organ in the human body and forms a protective barrier against the outside world. Its structure is extraordinarily adapted to protect the body from external factors (e.g., temperature, chemicals, and pathogens) and to maintain homeostasis [14].

Anatomically, it is divided into three layers: epidermis, dermis and hypodermis (also called the subcutaneous tissue), with different degrees of specialization within each layer (Fig. 1.3a) [14, 15].

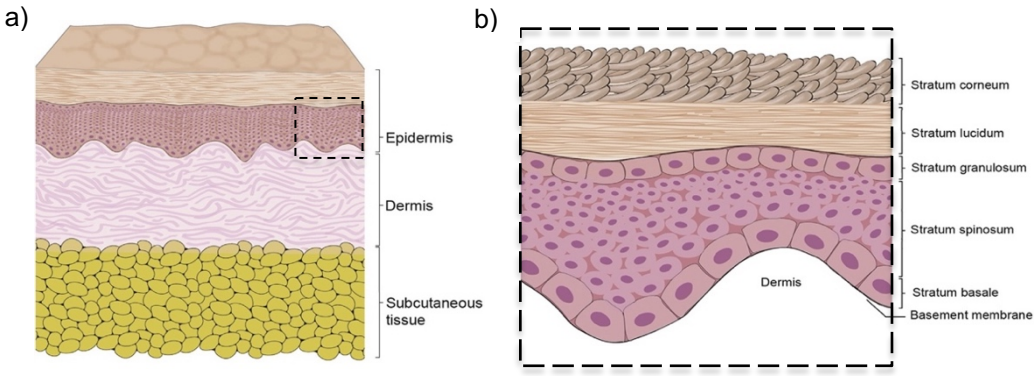

Figure 1.3 – (a) Diagram of the main layers of the human skin; (b) Structure of epidermis. Adapted from [14].

The epidermis is the most superficial and biologically active layer of the skin. It is composed mainly of keratinocytes and is divided into five layers: stratum corneum, stratum lucidum, stratum granulosum, stratum spinosum, and stratum basale (Fig. 1.3b). The stratum basale has progenitor cells, which differentiate into keratinocytes. Keratinocytes differentiate and mature as they move towards the surface of the skin (stratum corneum). This process results in keratinization, in which keratinocytes accumulate keratin. When the keratinocytes reach the

stratum corneum they are shed from the skin. The epidermis is a continually regenerating structure since the differentiation process takes approximately 30–40 days [14, 16].

Other cells are also found in the epidermis, including: (1) melanocytes, cells responsible for skin pigmentation and ultraviolet protection, (2) Langerhans cells, with a key role in the immune response of skin against pathogens, and (3) Merkel cells, essential for touch sensation [14, 16].

The dermis is separated from the epidermis by the basement membrane. It is an irregular connective tissue composed of blood and lymphatic vessels, oil and sweat glands, nerves, hair follicles, and fibrous tissue [14, 15]. The structure of this layer provides resistance and flexibility to the epidermis and support for vast vasculature, lymphatic system, and nerves [15]. It is mainly constituted by the extracellular matrix (ECM) with interconnected collagen fibrils, elastic fibers, proteoglycans, and glycoproteins. The predominant ECM component is collagen and the two major collagen found in the dermis are type I (80–90 %) and type III (10–20 %) [15, 17]. There are some types of cells within the connective tissue of the dermis, including: fibroblasts, endothelial cells, macrophages, and adipocytes. Fibroblasts are the principal cell type present in the dermis and are responsible for generating ECM and allowing the skin to recover from injury [16].

Below the dermis layer is the hypodermis, also called the subcutaneous tissue. It is the deepest layer of the skin and is composed by adipose cells, fibroblasts, macrophages, as well as bigger blood vessels and lymphatic vessels [14]. This tissue plays a particular role in adipocyte homoeostasis, thermoregulation, shock absorption, and water storage [14, 15].

Radiotherapy should always be a balance between destroying cancer and minimizing damage to the surrounding healthy cells. In fact, ionizing radiation acts preferentially in the cells that are actively dividing, such as cancer cells. However, cells from the basal layer of the epidermis are also considerably affected. Besides, when radiation passes through the skin to reach the tumor, all the normal cells in the area may become damaged. Thus, skin is one of the most affected organs in radiotherapy treatment [10].

1.4 – Wound Healing

In healthy skin, wound healing is a dynamic and complex process that can be divided into four phases, namely (1) homeostasis, (2) inflammation, (3) proliferation and (4) remodelling (Fig. 1.4) [18]. After skin injury, blood platelets stick to one another and to the wound site, and thrombin triggers the coagulation cascade, which forms a mesh preventing further bleeding. Besides, platelets play an important role in leukocyte recruitment and the initiation and progress of inflammation. The inflammatory phase is characterized by the recruitment of immune cells such as macrophages and neutrophils into the wound site, which will remove damaged and dead cells, bacteria and other pathogens or debris. Platelets and inflammatory cells release growth factors that recruit fibroblasts and endothelial cells into the wound, producing, that, collagen/granulation tissue and a new network of blood vessels, respectively. Subsequently, the epithelialization process occurs, in which epithelial cells migrate upwards to cover the defect. Finally, during the tissue remodelling phase, excess collagen fibers are degraded, and wound contraction begins to peak, resulting in scarring [18, 19].

Importantly, the skin is lubricated and slightly acidic (around pH 5.5–6) [20]. However, after a certain skin injury, the pH of the wound increase to pH values in the alkaline range (around

8–8.5). If the wound healing is functional, the pH of the wound decreases gradually, from pH values in the alkaline range to the pH of intact skin (5.5–6). However, if the pH values remain at a high level, the wound healing process will slow down or even stop [20].

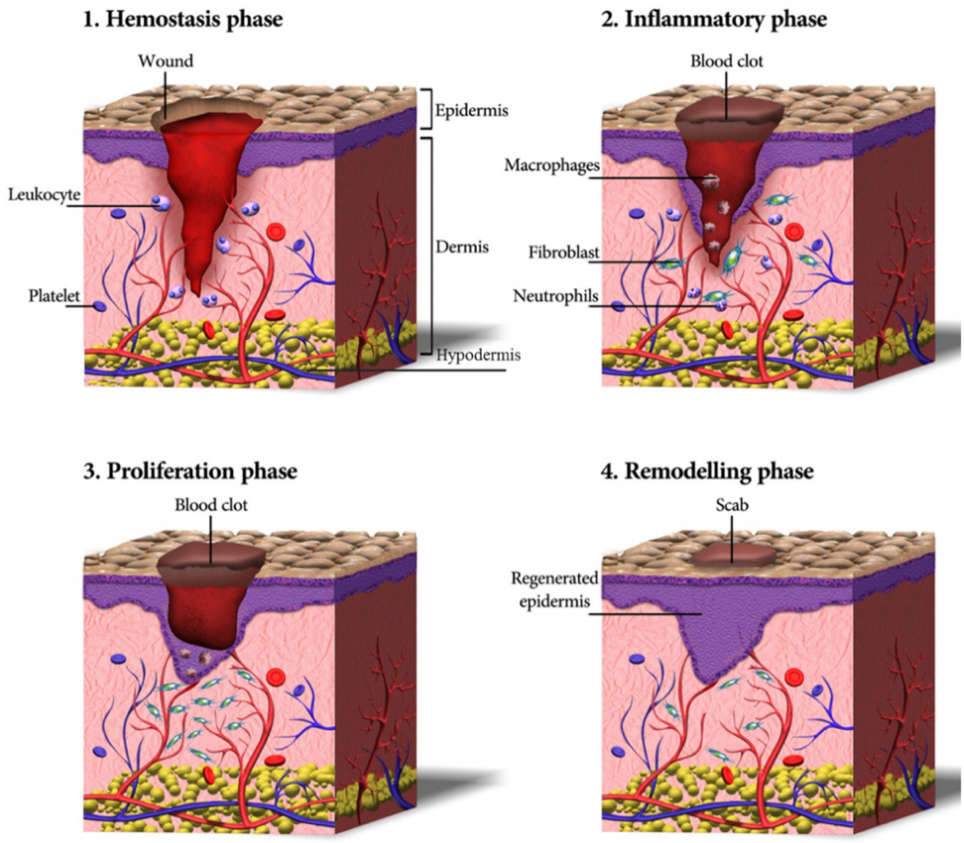

Figure 1.4 – Schematic representation of the process of wound healing. After injury, (1) blood platelets are activated to form a clot and recruit leukocytes. Then, (2) neutrophils and macrophages remove damaged and dead cells, bacteria, and other pathogens or debris. Next, (3) fibroblasts migrate, proliferate, and activate the angiogenesis process. Finally, (4) granulation tissue is formed, the extracellular matrix proteins are deposited to reconstitute the dermal tissue, and the epidermis is regenerated [18].

Normally, the human skin possesses high self-regeneration potential [18]. However, in case of deep injuries or skin defects, the skin healing does not happen spontaneously, requiring medical intervention. According to the types and stages of wounds, medical dressings can be applied to their surface to promote the healing process [18, 19].

In the case of radiotherapy, it is known that this treatment retards cell proliferation, decreases cytokine activity and collagen content, and can cause various histological skin changes such as a decrease in skin hydration and an increase in skin pH. As result, there is a delay in the wound healing process, impairing the skin's barrier function [13, 19], and can lead to RD development. Therefore, the use of a suitable dressing can also accelerate the wound healing process, healing in the management of RD [19]. In general, dressings are used to treat acute dermatitis because acute dermatitis might cause premature radiotherapy stoppage and, as a result, influence treatment outcome and overall survival rate. Although current studies show us that the use of wound dressings can improve acute RD, there is a lack of evidence-based, randomized, controlled trials comparing different types of these dressings [19]. More studies

should be done because there are many types of dressings with distinct properties, and different pathological types of wounds also have their own characteristics [19].

1.5 – Tissue Engineering - Hydrogels

Tissue engineering (TE) is a multidisciplinary discipline that aims to replace and/or regenerate previously damaged tissues/organs [21, 22]. Most TE approaches combine biology, biochemistry, physics, medicine, and materials science to achieve medical applications. There are several strategies of TE capable of restoring, retaining, and revitalizing lost tissues. Usually, the TE mechanism is based on the incorporation of three elements: (1) cells to synthesize the matrices of new tissue, (2) a biomaterial that provides the proper environment for cell attachment, proliferation, differentiation, and migration, and (3) biological signals (e.g., growth factors) that stimulate cells to regenerate damaged tissue [21, 22].

In recent years, tremendous progress has been made in the field of TE to develop new matrices for tissue regeneration. Among them, hydrogels are one of the possibilities with great potential to mimic the native skin microenvironment due to their excellent characteristics, such as biocompatibility, biodegradability, softness, hydrophilicity, and viscoelasticity [18, 19, 23-25].

Hydrogels are defined as a three-dimensional (3D) network formed by hydrophilic polymers, which can be physically or chemically crosslinked [25, 26]. These hydrophilic structures can mimic the properties of various tissues in the body due to their structural similarity to the ECM, and ability to restore the morphological characteristics and mechanical properties of damaged tissue [22]. Importantly, the hydrophilicity of this 3D network is due to the presence of hydrophilic functional groups in their polymeric structure, such as hydroxyl (−OH), carboxyl (−COOH), amino ($-NH_2$) and amide (−CONH) groups [21, 27].

Hydrogels can absorb and retain large amounts of water or other aqueous solutions (e.g., saline). The ability of a hydrogel to absorb and retain water is known as swelling behavior and water content, respectively [27]. Regarding the swelling behavior, hydrogels can swell until the osmotic forces that help to extend the polymer network are balanced by the elastic forces from the stretched segments of the polymer [25, 27]. Thus, they require a certain time to reach an equilibrium between the forces that allow the diffusion of water/physiological fluids into the hydrogel network, and the forces exerted by the polymer strands within the hydrogel [25, 27]. The swelling process of hydrogels can be controlled by two factors, (1) properties of the polymer forming the hydrogel (e.g., cross-linking density, hydrophilicity, hydrophobicity, concentration), and (2) properties of the swelling medium (e.g., ionic strength, pH, temperature) [25, 28]. When fully swollen, hydrogels show unique characteristics such as being soft and rubbery and having low interfacial tension with water and physiological fluids. These characteristics make them similar to ECM in living tissues [25].

The water content of hydrogels may vary in a wide range. In general, hydrogels with high water content (from 70 to 90 %) possess a degree of flexibility very similar to natural tissue [21, 28]. Furthermore, they maintain a physiologically moist environment that creates excellent conditions for cell proliferation and differentiation [28].

Hydrogels have several advantages when used as matrices for skin engineering, because their physicochemical parameters and mechanical properties are easily adjusted to desirable levels of an engineered skin substitute [29].

In a wound healing process, an ideal skin substitute should (1) act as a barrier to protect the wound from infection, (2) maintain hydration, (3) be permeable to gas exchange and water vapor, (4) provide support for cellular migration and proliferation, (5) be easily handled, (6) be non-adherent, (7) provide no local or systemic toxicity, (8) have adequate physical and mechanical properties, (9) be available and (10) at low cost [16, 24]. Furthermore, all skin substitutes need to satisfy the basic requirements of biocompatibility and biodegradability [18].

Several studies have shown that hydrogels can be used as wound dressings as they can accelerate the healing process [7, 19, 22-24]. The hydrogel-based wound dressings have shown (1) an extraordinary potential to absorb exudates from the wounds, (2) high water-swelling capacity while being non-water-soluble (i.e., swell readily without dissolving), (3) oxygen delivery capacity and (4) ability to protect the wound from external factors (e.g., microorganisms, temperature changes) [18, 26]. In fact, traditional wound dressings (e.g., gauze, and bandages) also provide a physiological barrier to prevent contaminations, meanwhile permitting exudate adsorption to maintain a dry environment at the wound site. However, modern wound dressings such as hydrogel-based wound dressings, can provide a moist environment that stimulates cell proliferation and differentiation, and consequently accelerate the healing process as well as help the cleaning of the necrotic tissue [28].

Owing to their exceptional hydration capacity, hydrogels keep the wound moist and play a positive role in cleaning the necrotic tissue. Moreover, a wound covered with a dressing can easily be replaced or monitored, as the hydrogels are usually non-adherent and transparent [19]. All these features point to the potential hydrogel therapeutic in the management of acute RD [5, 9, 19].

Hydrogels can be used as a permanent or temporary dressing to cover different wounds and improve their regeneration. Based on the polymer used for their synthesis, hydrogels can be divided into two different groups: natural and synthetic [18]. Natural polymers are mostly obtained from natural sources such as animals, vegetables, and microorganisms. Instead, synthetic polymers are synthesized and adjusted in a controlled mode to obtain certain physicochemical characteristics [24]. In medical applications, natural-derived polymers have some advantages when compared with synthetic ones, because they have biological properties (e.g., biocompatibility, biodegradability, biological activity) similar to the ECM of the tissues, making them appropriate for the substitution of natural ECM structural components. Additionally, these natural biomaterials share a chemical structure, rich in groups that can be blended with some elements, resulting in versatile materials suitable for several TE requirements. Unfortunately, natural polymers have high degradation rates, which are quite difficult to control. However, their derivatives are generally well tolerated by living organisms without triggering toxic reactions [24]. When compared with natural polymers, synthetic polymers are (1) biologically inert, (2) do not enclose impurities, (3) degrade in a controlled manner, and (4) have relatively low cost [24].

Both natural and synthetic polymers can be used in TE to fabricate hydrogels. However, natural polymers (e.g., alginate and collagen) have been some of the most commonly used polymers in wound healing applications [24, 29].

1.6 – Alginate and Collagen

Alginate (Alg) is an anionic biopolymer composed of (1–4) ß-D-mannuronic acid and α-L-guluronic acid residues linked either randomly or as homopolymeric blocks (Fig. 1.5) [30]. The residues are arranged into three types of polymer segments: (1–4) ß-D-mannuronic acid residues alone (-M-M- blocks), segments formed entirely of α-L-guluronic acid (-G-G- blocks) or segments formed of alternating ß-D- mannuronic acid and α-L-guluronic acid residues (-G-M- blocks) [31, 32]. The proportions and the sequence of M and G residues determine the physical properties and molecular weight of alginates [30, 31].

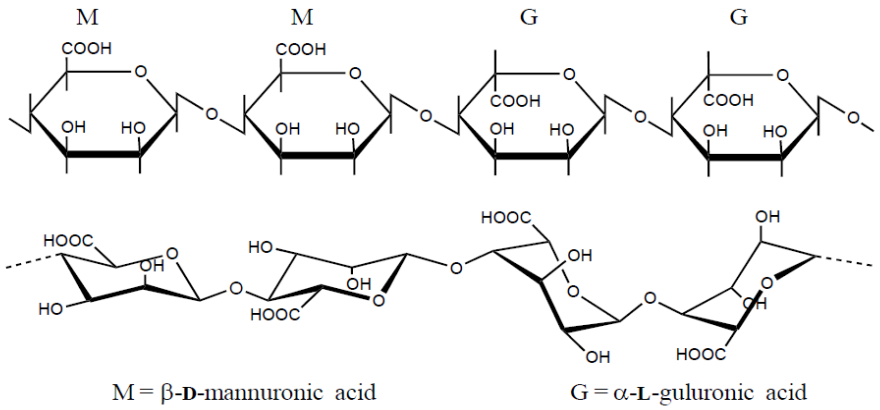

Figure 1.5 – Chemical structure of alginate. In this case, a segment of –MMGG– residues [30].

Alg is obtained from brown seaweed, as well as bacteria and it is widely used in several biomedical applications such as wound healing dressings [26, 31, 33, 34]. This natural polymer is an important biomaterial for wound healing due to its excellent properties: hydrophilicity, biocompatibility, non-toxicity, non-immunogenicity, biodegradability, hemostatic capabilities, resistance in acidic media, and relatively low cost [24, 30, 31, 35]. Alg can be used in the synthesis of materials for wound dressing, and these may have different formats, including hydrogels, films/membranes, nanofibers, foams, and topical formulations [31].

Alg hydrogel-based dressings can absorb wound exudates, maintain a physiologically moist environment, promote granulation tissue formation, and protect the wound site from bacterial infections [19, 24, 31].

Alg forms hydrogels in the presence of divalent ions, such as calcium ions (Ca^{2+}), which react preferentially with G-block regions of the polymer, through electrostatic interactions (Fig. 1.6) [26]. The gelation of Alg occurs when -G- block region chains align and cooperatively bind the divalent cations. The resulting configuration is known as the “egg-box structure” since one divalent ion binds to four G units [26, 32, 36, 37].

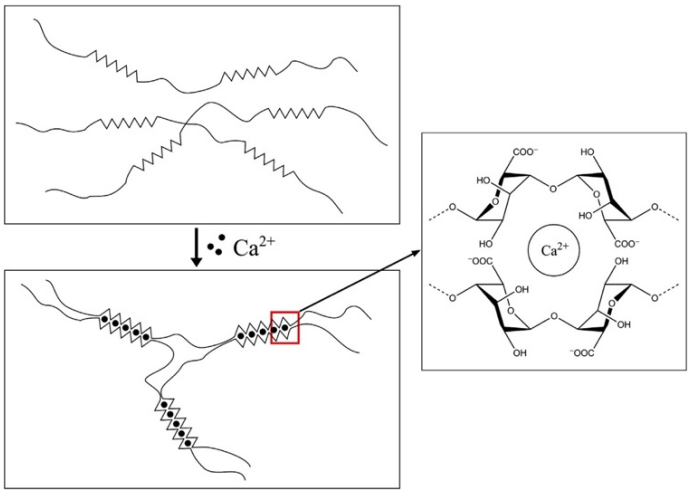

Figure 1.6 – Mechanism of ionic cross-linking of an alginate solution and calcium ions resulting in gel formation with characteristic egg-box structure [37].

Owing to the high affinity of divalent ions toward the G-blocks, the gel properties will be highly dependent on the M/G ratio (i.e., the ratio between M and G blocks) and the G-block length [38]. An Alg with a higher G content (low M/G ratio) tends to yield hydrogels with greater mechanical stiffness and strength than an Alg with a high M/G ratio [26, 38]. Importantly, since Alg is a natural biopolymer, the sequence of G and M blocks can vary significantly between the different sources of raw material [37].

The gelation process can also occur in the presence of trivalent ions such as aluminium (Al^{3+}) and iron (Fe^{3+}) and the binding intensifies, resulting in a more compact gel network when compared to divalent ions [27, 31].

Alg hydrogels can be formed by two different mechanisms: internal or external gelation [33]. These methods differ in how the crosslinking agent is introduced into the Alg network. For internal gelation, crosslinking ions are released in the interior of the Alg phase by controlled exposure, and the result is a homogeneous distribution of Alg in the hydrogel [37]. This internal crosslinking has been reported in the literature, and the results show that gels produced by internal gelation are less compact and more porous, and have higher release rates [37]. Differently, external gelation is a diffusion of crosslinking ions from the outside into the interior of an Alg phase (Fig. 1.7) [33, 37]. This external crosslinking produces inhomogeneous gels but with uniform thickness, different geometries, and good reproducibility [33]. Further, external gelation offers more rapid gelation, a smoother surface, and a denser structure than internal gelation [33, 36, 37].

The therapeutic efficacy of Alg hydrogel-based dressings can be influenced by several factors such as the (1) ratio of other polymers utilized in combination with Alg, (2) properties of crosslinkers used, (3) time, pH, temperature of crosslinking, (4) nature of excipients used, (5) incorporation of other particles (e.g., nanoparticles), and (6) antibacterial agents [31, 37].

Although Alg possesses excellent properties for TE applications, it lacks specific interaction with human cells. Therefore, Alg is often functionalized with cell adhesion ligands such as the tripeptide Arginine-Glycine-Aspartate (RGD). RGD is a recurrent cell-recognition ligand in ECM that binds integrins to the membrane proteins of different cell types. This cell ligand is present in collagen fibrils in human tissues. Accordingly, the composite hydrogel of alginate and collagen may provide the adhesion sites for cell attachment and proliferation [39].

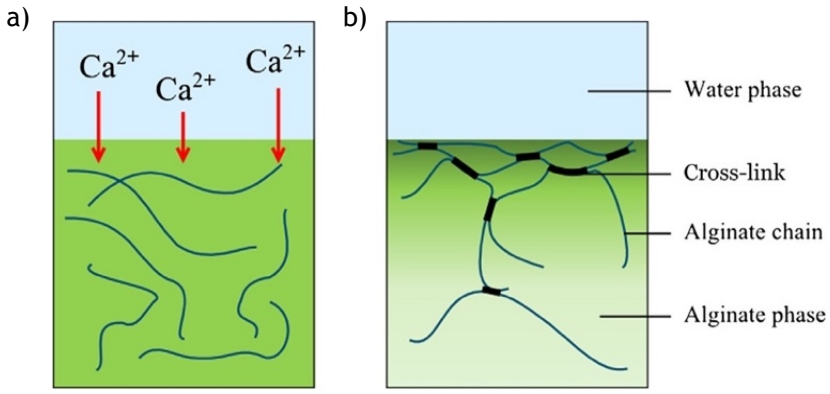

Figure 1.7 – Schematic representation for the formation of alginate hydrogel via external gelation. (a) Cations (Ca^{2+}) diffuse from the exterior of the alginate phase to the interior. (b) A hydrogel is formed with a higher alginate and Ca^{2+} concentration at the surface. Adapted from [37].

Collagen (Col) is one of the main structural elements of the ECM of tissues and is very important for cell recognition, attachment, proliferation, and differentiation [36, 39]. Further, it is a fundamental component to maintain the structure and biological integrity of connective tissues [40].

Col is a protein containing three polypeptide chains (α-chains), each of which is characterized by an amino acid repeating sequence [Glycine-X-Y]n, where X and Y are occupied by proline and its hydroxylated form, hydroxyproline, respectively [40, 41]. The three α-chains are organized in a triple-helical conformation that forms a filament known as Col fibril. Several Col fibrils are incorporated into a structure called Col fiber (Fig. 1.8) [40, 42].

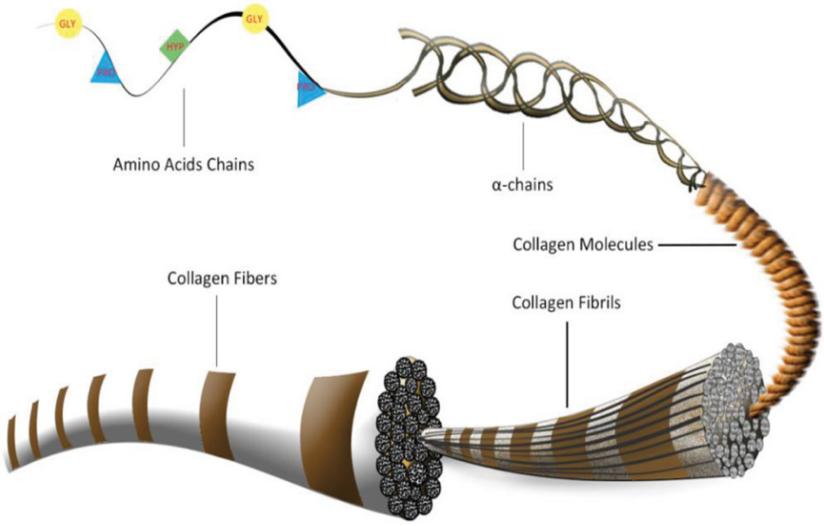

Figure 1.8 – Schematic representation of the four-level structure of a collagen fiber. From [42].

To date, there are 29 Col types numbered in roman numerals (I to XXIX), and all types are characterized by the typical triple-helical structure [40-43]. This Col family can be subdivided into (1) fibril-forming collagens, (2) fibril-associated collagens, (3) beaded-filament forming collagens, (4) basement membrane collagens, (5) transmembrane collagens, (6) collagens forming hexagonal networks and anchoring fibrils, and (7) multiplexins [44]. The fibril-forming

collagens are the most abundant collagens subfamily, with about 90 % of the total Col. The fibril-forming collagens are type I, II, III, V, XI, XXIV and XXVII. Among them, type I collagen (ColI) is the most prevalent in the human body, is particularly important in bone tissue, skin, and tendon, and it is the best-studied [40, 44, 45]. The collagen fibrils are important for cell attachment and tissue repair, and their formation is basically a self-assembly process (i.e., one that is determined by the intrinsic properties of the Col molecules) [40].

The high prevalence of Col in human tissues and its inherent properties (e.g., good cell recognition and biocompatibility, weak immunogenicity, biodegradability, and ability to form 3D matrices) makes it a natural choice as raw material for TE [24, 40, 43]. The major hurdle that restricts the widespread application of Col is its poor mechanical properties. To improve their mechanical properties, Col can be incorporated with other materials, such as Alg. In fact, it is reported that Col in the combination with Alg not only enhances the mechanical properties of the composite hydrogel but also tunes their stiffness [43].

Col can be obtained from different sources such as animals, marine organisms, and synthetic sources [43]. Several studies show that Col molecules can be incorporated in scaffolds, such as Alg matrices, to recreate Col fibers functions [35, 36, 39, 41]. Further, Col-based scaffolds have the capacity to replace the native function of ECM and can play an important role in the wound healing process [24, 35, 46].

Chapter 2

Objectives

The main objective of this work is the development of a hydrogel-based dressing for acute radiodermatitis treatment. It is expected that it will restore the morphological characteristics of damaged skin, promoting rapid wound healing.

Thereby, alginate-collagen hydrogels will be produced and characterized in terms of morphology, chemical composition, swelling behavior, water content, pH-responsive behavior, and protein adsorption for radiodermatitis treatment. Furthermore, human dermal fibroblast cells under and without radiation treatment will be cultured to assess the *in vitro* cytocompatibility and regenerative effect of the hydrogels.

Chapter 3

Materials and Methods

3.1 Preparation of the Alg-ColI hydrogels

Initially, stock solutions of Alg and ColI (Fig. 3.1a) were prepared: a) Alg at 4 % (w/v) solution was obtained by dissolving sodium Alg (Sigma-Aldrich, China) powder in distilled water, under constant stirring, at room temperature (RT), and b) ColI at 0.5 % (w/v) solution was prepared by swelling bovine ColI flakes (Sigma-Aldrich, USA) into 0.01 M hydrochloric acid pH 2.1 (VWR Chemicals BDH®, Belgium) overnight at 4 °C, and homogenized at 12.4 rotations per minute (rpm) using an ULTRA-TURRAX® IKA for 3 h to break down the ColI flakes to individual ColI fibrils.

Posteriorly, nine hydrogel formulations (Table 3.1) at different ColI concentrations (0, 0.125 and 0.25 %), temperatures (RT and 37 ºC) and incubation times (0, 12 and 24 h) were produced by external gelification, using calcium chloride dihydrate ($CaCl_2$) at 0.25 M (Sigma-Aldrich, Germany). Briefly, Alg at 4 % (w/v) and ColI at 0.25 and 0.5 % (w/v) solutions were mixed in a 1:1 ratio (Fig. 3.1b). After homogeneity, the resulting mixtures were placed into a mold (1 cm × 1 cm × 1 cm) (Fig. 3.1c) at RT without incubation time and at 37 °C for 12 and 24 h to trigger ColI fibril formation (Fig. 3.1d). Subsequently, gelification process was performed for 30 min under constant stirring using a plate shaker, to form hydrogels (Fig. 3.1e). Afterwards, hydrogels were rinsed five times with distilled water (Fig. 3.1f) and kept at 4 °C.

Table 3.1 — External conditions used for preparation of Alg-ColI hydrogels.

Hydrogel Formulation	Abbreviation	Temperature [°C]	Incubation time [h]
Alg 2 % (control)	Alg	RT	0
Alg 2 %-ColI 0.125 %	Alg-ColI0.125		
Alg 2 %-ColI 0.25 %	Alg-ColI0.25		
Alg 2 % (control)	Alg	37	12
Alg 2 %-ColI 0.125 %	Alg-ColI0.125		
Alg 2 %-ColI 0.25 %	Alg-ColI0.25		
Alg 2 % (control)	Alg	37	24
Alg 2 %-ColI 0.125 %	Alg-ColI0.125		
Alg 2 %-ColI 0.25 %	Alg-ColI0.25		

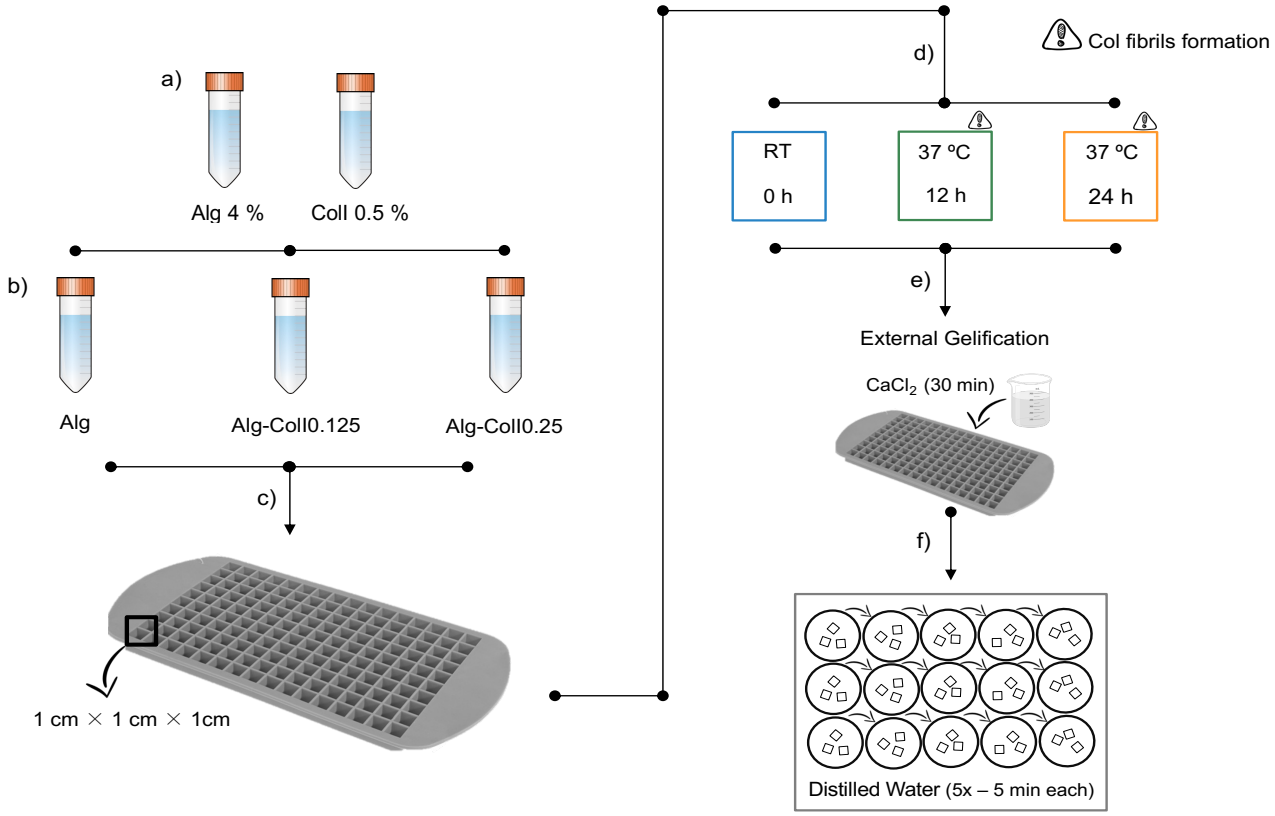

Figure 3.1 – Schematic of the step-by-step preparation process of the Alg and Alg-Coll hydrogels. (a) Stock solutions of Alg 4 % and Coll 0.5 % were used to obtain (b) pre-gelled solutions of Alg (control), Alg-Coll0.125, and Alg-Coll0.25. After homogeneity, (c) the resulting mixture was placed into a mold (1 cm × 1 cm × 1 cm) (d) at RT without incubation time and at 37 °C for 12 and 24 h, to trigger Coll fibril formation. (e) A crosslinking agent was placed over Alg and Alg-Coll gels, and (f) the resulting hydrogels were rinsed.

3.2 Characterization of the Alg-Coll hydrogels

3.2.1 Morphology

Digital images of hydrogels were obtained using a Wireless EP50 Camera – Stereomicroscope SZX10 (OLYMPUS, Germany), with a magnification of 6.3x.

The surfaces morphology of the freeze-dried hydrogels was evaluated by Scanning Electron Microscopy (SEM), using a FEI Quanta 400 FEG / ESEM microscope (FEI, USA) with an accelerating voltage of 15 kV. Previously, the samples were fixed to the surface of a specific sample holder using a carbon ribbon for sticking the sample. The samples were then coated (SPI-Module) with a thin layer of gold/palladium in an argon atmosphere.

The hydrogels matrixes were characterized by Transmission Electron Microscopy (TEM), using a JEOL JEM 1400 Electron Microscope (JEOL Ltd., Japan), with a STEM detector and EDS system. The samples were initially fixed in 2.5 % glutaraldehyde and 2 % paraformaldehyde in 0.1 M sodium cacodylate, and washed 3 times for 5 min each, in 0.1 M sodium cacodylate buffer. Then, the samples were post-fixed with 1 % osmium tetroxide and 1.5 % potassium ferrocyanide in 0.1 M cacodylate buffer (pH 7.2) for 1 h. Posteriorly, the samples were incubated with 1 %

uranyl acetate in water overnight at 4 °C, and dehydrated in ethanol (7 times for 10 min each) and propylene oxide (3 times for 10 min each). After fixation and, dehydratation, the samples were included in resin (propylene oxide and EPON) for 48 h at 55 °C. Ultrathin sections (40−60 nm thick) were stained with uranyl acetate and lead citrate and examined using a JEOL JEM 1400 Electron Microscope with an accelerating voltage of 80 kV.

3.2.2 Histochemical analyses

The samples were initially fixed using 10 % Neutral Buffered Formalin overnight. After fixation, the samples were included in paraffin and 3 µm sections were obtained and stained with Picro-Sirius Red. Briefly, sections were deparaffinized and rehydrated, stained for 3 min in Gill's Hematoxylin and tap water washed for 6 min. Then, sections were stained in Picro-Sirius Red solution for 1 h and differentiated with acidified water for 30 sec. After a quick dehydration in 96 % and 100 % ethanol, sections were mounted in Entellan.

The images were digitally recorded using an Olympus CX31 light microscope equipped with a DP25 camera and U-CMAD3 adapter (Olympus, Japan), and an inverted fluorescence microscope, Axiovert 200M (Zeiss, Germany), in order to assess the ColI formation and maturation, respectively.

3.2.3 Chemical Profile

Chemical characterization was performed using Attenuated Total Reflectance – Fourier Transform Infrared (ATR-FTIR) spectroscopy, with a Perkin – Elmer 2000 FTIR spectrometer (Perkin-Elmer, USA). Alg-ColI solutions (Fig. 3.2a) and Alg-ColI hydrogels (Fig. 3.2b) were analyzed at a spectral resolution of 4 cm−1 in the range of 4000 to 400 cm-1, and 32 scans were accumulated per sample. Three measurements were done per sample.

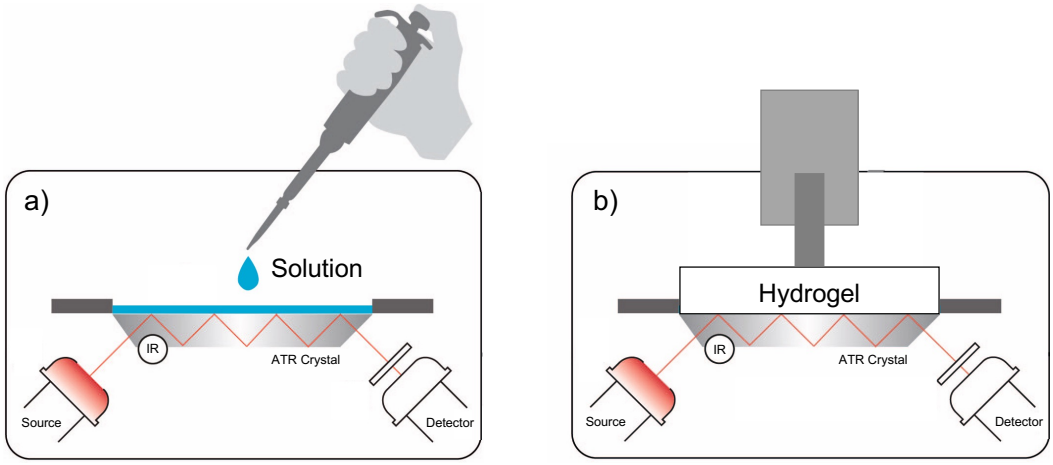

Figure 3.2 - FTIR procedure for (a) liquid and (b) solid samples. ATR-FTIR spectra for liquid samples (Alg and ColI solutions) were obtained directly from drying a small drop on the ATR crystal. Whereas solid

samples (Alg and Alg-ColI hydrogels) were analyze applying a force on the equipment handle to achieve good contact with the ATR crystal.

3.2.4 Swelling Behavior

The swelling behavior of hydrogels was evaluated using a gravimetric method [47]. Briefly, the hydrogels were immersed in phosphate-buffered saline (PBS, 138 mM NaCl, 2.7 mM KCl, Sigma-Aldrich) pH 7.4 and incubated at 37 °C for 3, 12, and 24 h. At each time-point, the hydrogels were taken out, put on a filter paper to remove liquid excess on the surface, and immediately weighed. For all samples, the equilibrium swelling ratio was obtained after 12 h of incubation. The measurements were continued until reaching the constant weight. The equilibrium swelling ratio was calculated by the following equation:

$$Swelling\ ratio\ (\%)\ = (W_a - W_b)/W_b \times 100\ , \tag{3.1}$$

where, W_b and W_a are the weight of the hydrogel before and after immersion, respectively. The measurements were performed in quintuplicate (n = 5) for each experimental condition, and the results were taken as the mean values of measurements.

3.2.5 Water Content

The water content of hydrogels was also determined by the gravimetric method [47]. Briefly, the freeze-dried samples were firstly weighed and posteriorly immersed in PBS at pH 7.4. After immersion, all samples were incubated at 37 °C for 24 h. During the incubation period, the weights of hydrogels were recorded at 3, 12, and 24 h. At each time-point, the hydrogels were taken from the PBS solution, and the excess surface water was slightly removed by filter paper. The equilibrium was obtained after 12 h of incubation. The water content was calculated by the following equation:

$$Water\ Content\ (\%)\ = (W_w - W_d)/W_w \times 100\ , \tag{3.2}$$

where, W_w and W_d are the wet and dried weights of the hydrogels, respectively. The assessment was performed in triplicate (n = 3) for every sample, and the results were taken as the mean values of measurements.

3.2.6 Influence of pH on the stability of the Alg-ColI hydrogels

To evaluate the effect of pH, the hydrogels were immersed in universal buffer 1x (150 mM KCl, 10 mM KH_2PO_4, 10 mM $Na_3C_6H_5O_7$, 10 mM H_3BO_4) at different pH values (pH 5.5, 7.4 and 8) and kept at 37 °C for 3, 12, and 24 h. After incubation, hydrogels were taken out, put on a filter paper, and immediately weighed. The structural behavior of the hydrogels at different pH values was determined by the quantification of the weight alteration ratio following equation (3.1). All experiments were conducted in triplicate, and the results were taken as the mean values of measurements.

3.2.7 Influence of proteins on the stability of the Alg-ColI hydrogels

The potential effect of proteins on the integrity of hydrogels was evaluated through immersing samples in alpha-minimum essential medium (α-MEM) with and without fetal bovine serum (FBS, 10 % v/v, Gibco, USA). After immersion, samples were incubated at 37 °C for 1, 3, and 7 days. For each time-point, samples were weighted as previously described. The structural behavior of the hydrogels in α-MEM with and without FBS was determined by the quantification of the weight alteration ratio following the equation (3.1). The medium was replaced every 3 days to maintain the initial volume. Hydrogels immersed in α-MEM without FBS were used as controls. For each experimental condition, the measurements were performed in triplicate, and the results were taken as the mean values of measurements.

3.3 Cell Culture

The cell culture was performed using primary Human Dermal Fibroblasts (HDF) cells (Coriell Institute, USA).

HDF cells were cultured in α-MEM supplemented with 10 % (v/v) FBS, 100 IU/mL penicillin, 100 µg/mL streptomycin, and 2.5 µg/mL amphotericin B (all reagents from Gibco, USA), at 37 °C in a humidified atmosphere of 5 % CO_2. The medium was replaced twice a week. At an 80 % confluency, cells were washed twice with PBS and detached using TrypLE™ Express (Gibco, Denmark). Cells were then resuspended in culture media and collected to centrifuge (1200 rpm for 5 min). The obtained pellet was resuspended in culture media and a cell suspension of 1x104 cells/cm2 was seeded in 24-well plates (SPL Life Sciences, Korea) and incubated for 24 h, for posterior evaluation of: 1) the *in vitro* cytocompatibility of Alg and Alg-ColI hydrogels; 2) the influence of radiation in metabolic activity and cell proliferation; 3) the regenerative effect of

Alg and Alg-CoII hydrogels on irradiated cells, and 4) the cell cytoskeleton and morphology of irradiated cells (Fig. 3.3).

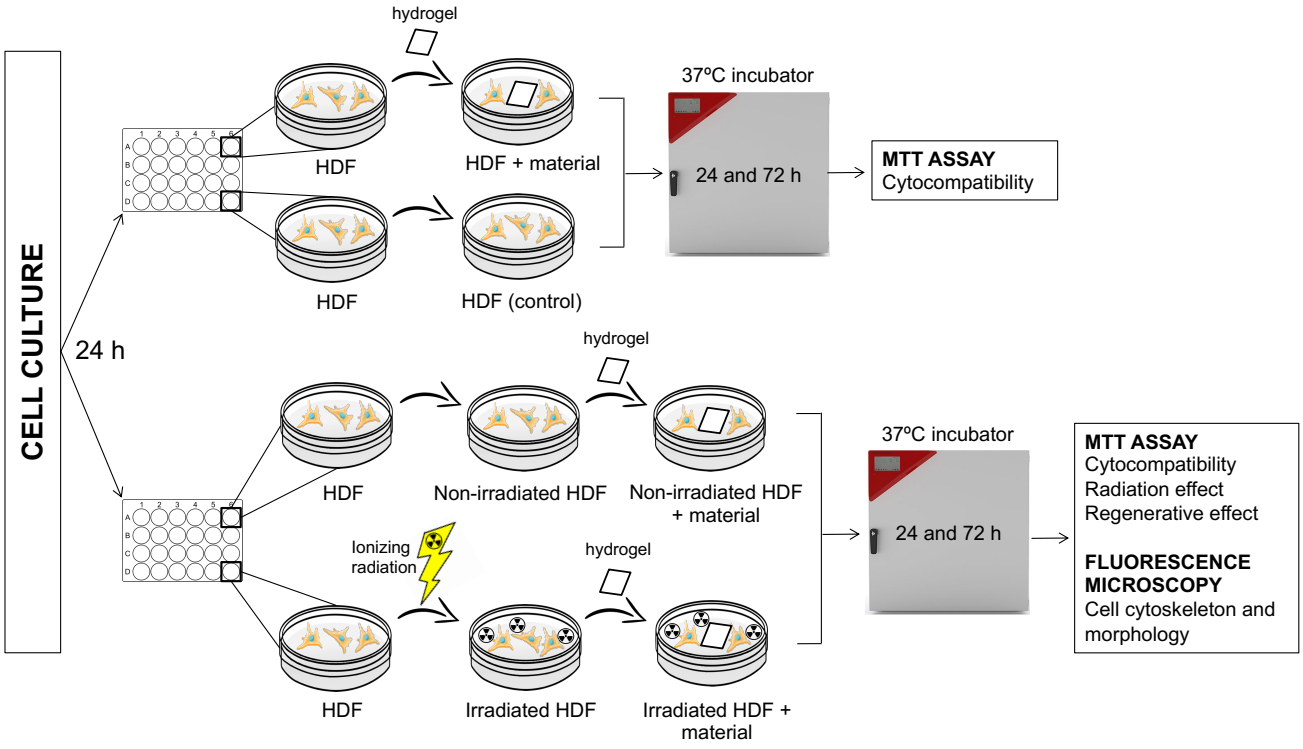

Figure 3.3 – Schematic representation of the cell culture experiments.

3.3.1 *In vitro* cytocompatibility of Alg-CoII hydrogels

3.3.1.1 Metabolic activity and cell proliferation

After seeding (section 3.3), the hydrogels were placed over the cell monolayers and further incubated at 37 °C for 24 and 72 h (see Fig. 3.3). Cells cultured in the absence of the hydrogels were used as controls. At each time-point, metabolic activity and cell proliferation were evaluated using the MTT assay, which is based on the reduction of 3-(4,5-Dimethylthiazol-2-yl)-2,5-Diphenyltetrazolium bromide (yellow) to a violet-blue formazan product by metabolic active cells. Briefly, cultures were incubated with 10 % MTT solution (5 mg/mL, Sigma-Aldrich, USA) for 3 h at 37 °C. After the incubation period, the culture medium was removed, and the formazan salts were dissolved with dimethyl sulfoxide (DMSO, Panreac, Germany) for 15 min at RT. The absorbance values were measured at λ = 550 nm in a microplate reader (Synergy HT, Biotek, USA).

The influence of radiation on the cell metabolic activity, and the regenerative effect of Alg and Alg-CoII hydrogels on irradiated cells were also evaluated using the MTT assay. After seeding (section 3.3), the cell monolayers were irradiated according to the previously reported methodology [48], at the Instituto Português de Oncologia do Porto. Briefly, cells were irradiated at RT with a 6-MV photon beam produced by a Varian DHX Medical Linear Accelerator

(Varian Medical Systems, USA). The cell culture plates were centered with the irradiation field, exposed at a source-surface distance of 98 cm for a field size of 25 x 25 cm, and irradiated with a daily dose of 2 Gy and dose rate of 600 cGy/min. Following irradiation, Alg and Alg-ColI hydrogels were placed over irradiated cell monolayers and further incubated at 37 °C for 24 and 72 h (Fig. 3.3). Non-irradiated cell cultures, and equally manipulated, were used as controls. At each time-point, the biologic response was evaluated in terms of metabolic activity and cell proliferation.

3.3.1.2 Immunofluorescence analysis of irradiated cells

Cell monolayers which were irradiated, exposed to hydrogels and posteriorly, incubated at 37 °C for 24 h, were characterized by fluorescence microscopy after immunostaining for F-actin cytoskeleton and nucleus. Firstly, cells were washed with PBS and fixed with formaldehyde 3.7 % for 15 min. Then, cells were permeabilized with 0.1 % Triton X-100 in PBS (15 min, RT) and incubated with 1 % bovine serum albumin (BSA, 30 min, RT) to reduce non-specific coloring. Cultures were stained for F-actin cytoskeleton with Alexa Fluor® 488 (1:150, 20 min, Enzo, USA), and nucleus with Hoechst 33342 (8 µg/mL, 15 min, Enzo, USA). Images were obtained with a Celena S digital imaging system (Logos Bio-systems, South Korea).

3.4 Statistical Analysis

All experiments were performed in triplicate as independent experiments. The results were represented as mean ± standard deviation (SD). The experimental data were performed using Microsoft Office Excel 2016. Statistical significance ($p < 0.05$) was determined using a two-tailed Student's T-test, assuming unequal variance.

Chapter 4.

Results and Discussion

4.1 Characterization of the Alg-ColI hydrogels

4.1.1 Morphology

Figure 4.1 presents digital images of Alg-ColI hydrogels obtained via external gelation, Overall, the hydrogels showed a tightly knit and smooth surface, and a blackened coloring proportional to the amount of ColI added (Fig. 4.1), regardless of the temperature (RT and 37 °C) or incubation time (0, 12 and 24 h). Regarding Alg hydrogels (controls), these exhibit a homogenous surface, while Alg-ColI hydrogels revealed a heterogeneous surface, with black dots uniformly scattered over the hydrogels' surface. These black dots are more prominent on Alg-ColI0.25 hydrogels, as expected.

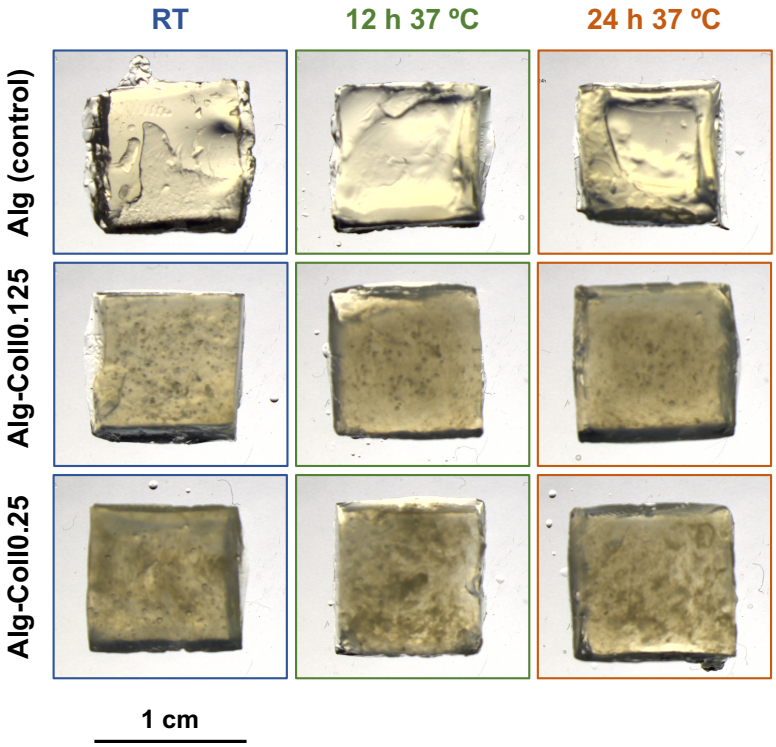

Figure 4.1 - Digital images of hydrogels composed with Alg and ColI at 0.125 or 0.25 %, produced at different temperatures (RT and 37 °C) and incubation times (0, 12 and 24 h). Alg hydrogels (with and without incubation time), were used as controls. The scale bars correspond to 1 cm.

The structure and morphology of freeze-dried hydrogels are shown in figure 4.2. Through SEM analysis, it was shown that the temperature (37 ºC) and incubation time (12 and 24 h) appear to induce an increase of grooves (ColI fibril formation) on Alg-ColI samples, which was significantly higher on Alg-ColI samples incubated for 24 h at 37 °C. Furthermore, SEM images showed that the ColI fibrils formation was apparently high on samples with more ColI concentration, i.e, on Alg-ColI0.25 surfaces compared to AlgColI0.125, as expected (Fig. 4.2).

Independently of temperature (RT and 37 °C) and incubation time (0, 12 and 24 h), Alg hydrogels (controls) presented a smooth surface, whereas Alg-ColI hydrogels (AlgColI0.125 and Alg-ColI0.25) presented grooves and stretch marks well-embedded throughout the Alg matrix (pointed by arrows in Fig. 4.2), which were more prominent on Alg-ColI0.25 hydrogels. Baniasadi and Jolandan found identical grooves and stretch marks on the surface of Alg hydrogels [39], and that was caused by ColI fibrils formation on the surface of the hydrogels, being also proportional to ColI concentrations used.

The present work also studied the influence of temperatures (RT and 37 ºC) and incubation times (0, 12, and 24 h) on ColI fibrils formation. From SEM analysis, it was shown that the temperature (37 ºC) and incubation time (12 and 24 h) appear to be induced the increase of ColI fibrils (grooves and stretch marks, pointed by arrows in Fig. 4.2) on Alg matrix, especially on the Alg-ColI hydrogels pre-incubated at 37 °C for 24 h.

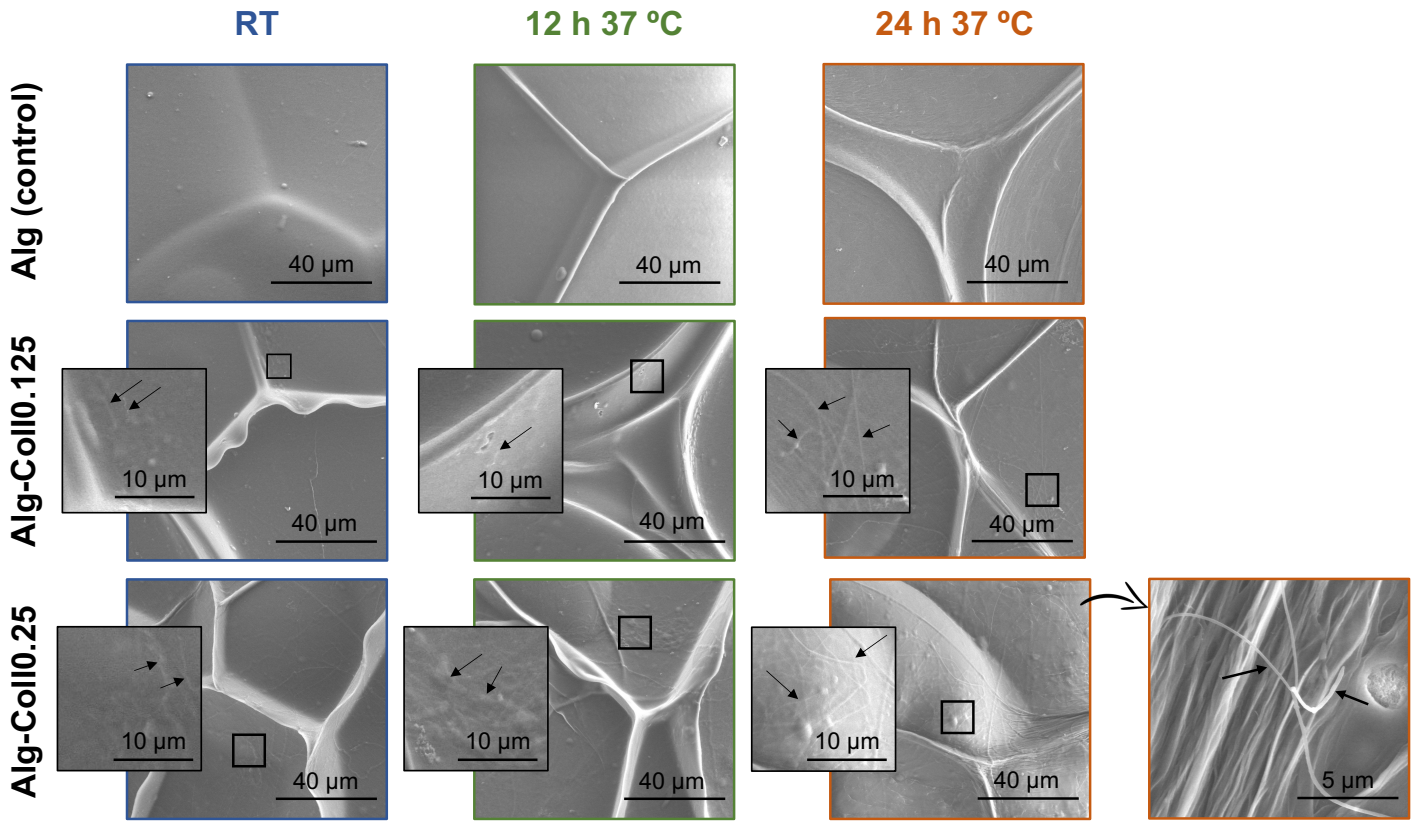

Figure 4.2 - SEM micrographs of morphology and structure of Alg and Alg-ColI hydrogels. The presence of ColI fibrils is pointed by arrows. Alg hydrogels (with and without incubation time) were used as controls. The scale bars correspond to 5, 10 and 40 µm.

With the purpose to confirm the presence and formation of ColI fibrils on the Alg matrix, TEM analysis was performed (Fig. 4.3). TEM analysis allowed to characterize the hydrogels matrix and confirm the presence ColI fibrils in the Alg network. Regarding the Alg hydrogels (controls), it was shown that the Alg matrix displayed dark wires which are the Alg clusters alternately linked in a continuous network, and grey zones occupied by water (Fig. 4.3), regardless of temperature and incubation time. Concerning Alg-ColI hydrogels, striated and elongated structures (ColI fibrils) were observed within the Alg matrix, namely in hydrogels pre-incubated at 37 ºC for 12 and 24 h. It should be noticed that the pre-incubation at 37 ºC induced a higher ColI fibrils formation on Alg-ColI hydrogels compared to Alg-ColI hydrogels produced at RT. Besides, it was shown that Alg-ColI hydrogels pre-incubated at 37 °C for 24 h appear to contain more ColI fibrils compared to Alg-ColI hydrogels pre-incubated at 37 °C for 12 h (Fig. 4.3). Furthermore, hydrogels with 0.25 % of ColI showed higher content of ColI fibrils than Alg-ColI0.125 hydrogels, as expected.

SEM (Fig. 4.2) and TEM (Fig. 4.3) data provide direct evidence that temperature (37 °C) and incubation time (12 and 24 h) led to an increase of ColI fibrils in the samples. These data are in accordance with a study performed by Moxon et al, where the authors showed that the incubation of Alg-ColI solutions at 37 °C for 4 h, prior to gelification, also led to ColI fibrils formation in the Alg network [49].

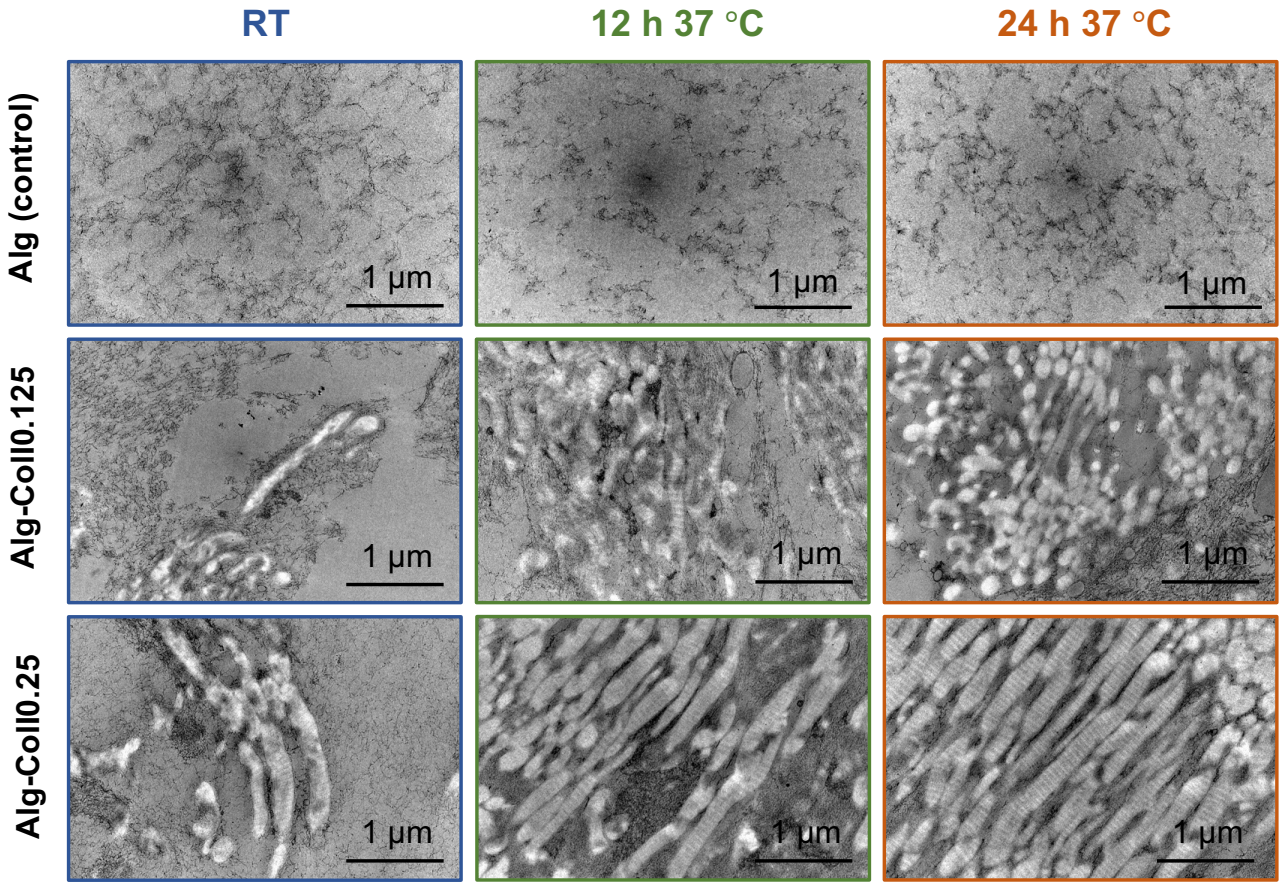

Figure 4.3 - TEM imagens of the matrix of Alg and Alg-ColI hydrogels. Alg hydrogels (controls) displayed dark wires in Alg matrix which are a fibril-like network, and grey zones occupied by water. Alg-ColI hydrogels highlighted the present of striated ColI fibrils within the Alg matrix, namely in hydrogels pre-incubated at 37 ºC for 12 and 24 h.

4.1.2 Histochemical analyses

Histochemical analysis of hydrogels, stained with Picro-Sirius Red, was performed in order to assess the ColI formation (Fig. 4.4) and maturation (Fig. 4.5). The images were captured with an Olympus CX31 light microscope equipped with a DP25 camera and U-CMAD3 adapter (Fig. 4.4) and an inverted fluorescence microscope, Axiovert 200M (Fig. 4.5).

Picro-Sirius Red stain is a selective histochemical method suitable for both morphological and semiquantitative detection in paraffin-embedded sections of fibrillar Col networks. Picro-Sirius Red is a strong, linear anionic dye comprising six sulfonate groups that can associate along cationic Col fibers, and enhance their natural birefringence under cross-polarized light. Thus, under polarized light, fibrillar Col networks can appear stained by green, red or yellow, depending on their polymerization degree and 3D organization [50-52], and are easily differentiated from the black background. This histochemical staining allowed thus distinguished mature and immature Col fibrils by colour, where immature ones appear stained green and mature at red [50-53].

Regarding the ColI formation (Fig 4.4), only Alg-ColI hydrogels revealed elongated structures stained red, the ColI fibrils (pointed by arrows in Figure 4.4), as expected. Alg-ColI hydrogels pre-incubated at 37 ºC for 24 h showed more prominent ColI fibrils formation compared to hydrogels pre-incubated at RT or at 37 ºC for 12 h. Besides, it was observed a higher content of ColI fibrils on Alg-ColI0.25 hydrogels than on Alg-ColI0.125 hydrogels (Fig. 4.4). These results showed that the pre-incubation of Alg-Col hydrogels at 37 ºC for 24 h has a positive impact on ColI fibrils formation on Alg matrix, as reported by Rivero et al, [52].

Regarding ColI maturation (Fig. 4.5), immatures ColI fibers (stained at blue-green) were observed on Alg-ColI hydrogels produced at RT, whereas, Alg-ColI samples pre-incubated at 37 °C for 12/24 h contained predominantly mature fibers (stained at pink-red). Ovchinnikova et al. [51] showed histological images stained by Picro-Sirius Red, where mature ColI fibers appear orange-red and immature ColI fibrils green under polarized light.

These findings suggest that the temperature (37 ºC) and incubation time (24 h) result in samples with a higher content of mature ColI fibers which could be important to promote cell adhesion and proliferation[40, 51].

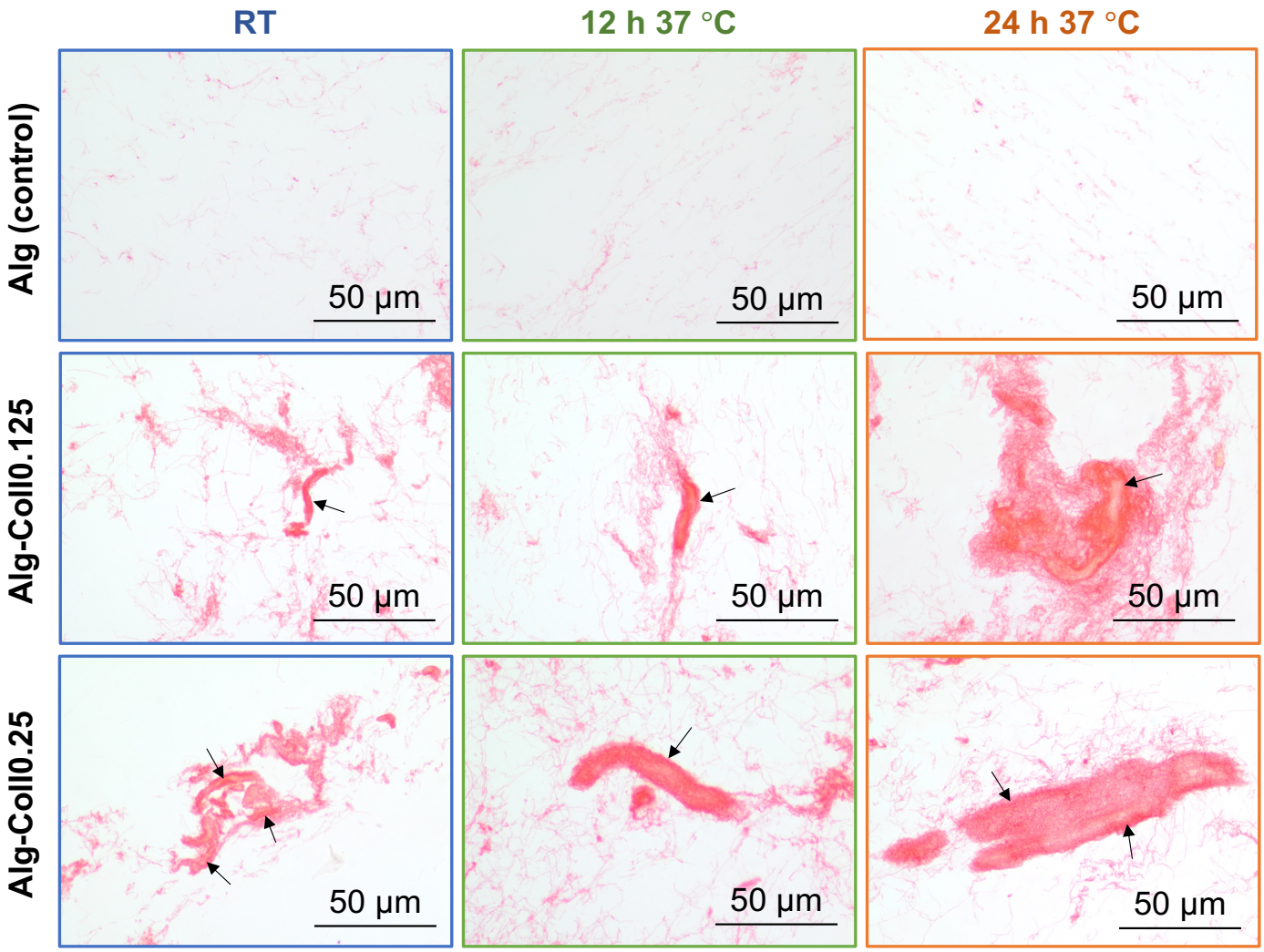

Figure 4.4 - Histological images of Alg and Alg-Coll hydrogels produced at different temperatures (RT and 37 °C) and incubation times (0, 12 and 24 h), stained with Picro-Sirius Red. The imagens were captured with Olympus CX31 light microscope equipped with a DP25 camera and U-CMAD3 adapter (Olympus, Japan). Under standard light, Picro-Sirius Red staining marks the Coll fibrils at red. All images were taken at 40X magnification and scale bars correspond to 50 µm.

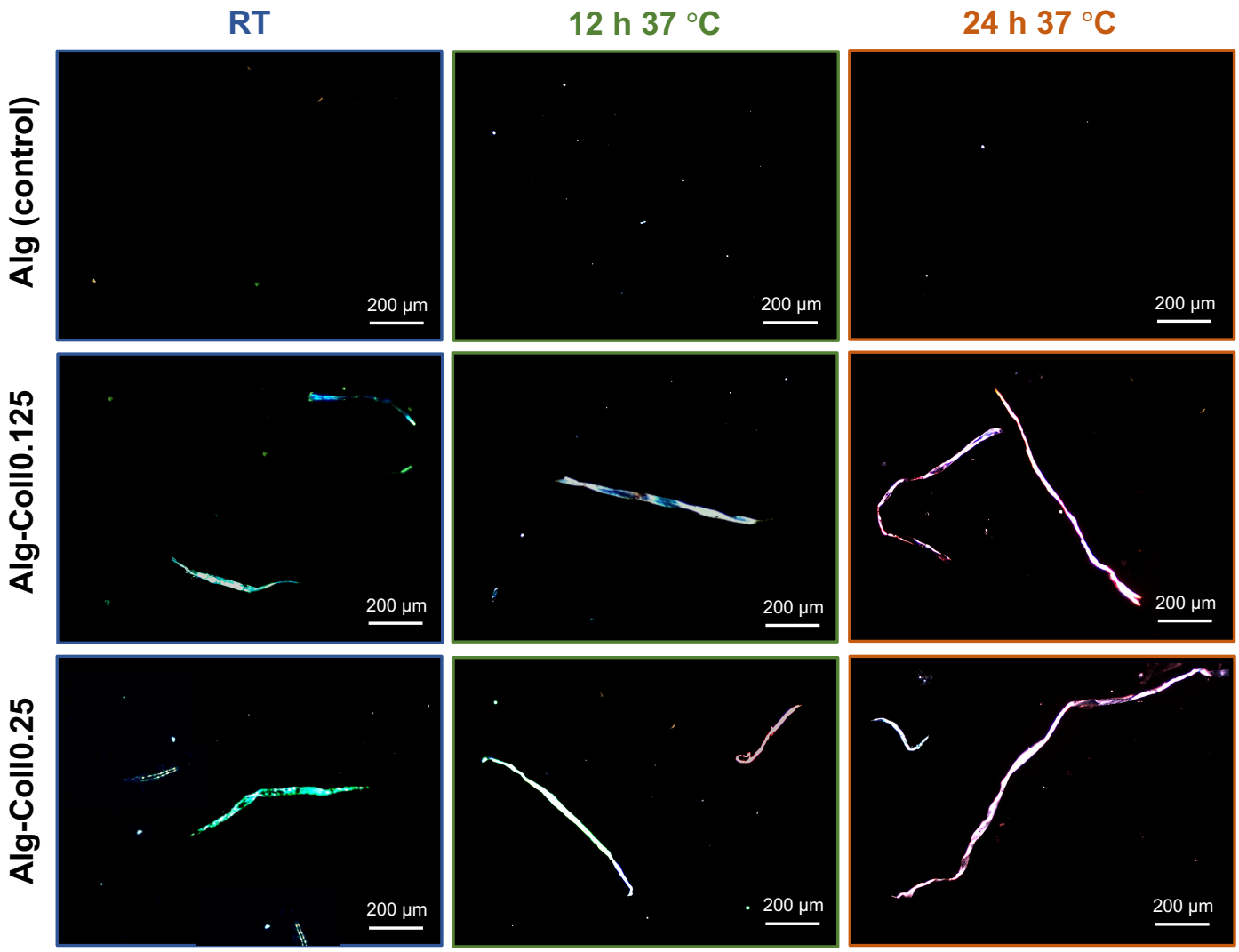

Figure 4.5 - Immunofluorescence images of Alg and Alg-ColI hydrogels produced at different temperatures (RT and 37 °C) and incubation times (0, 12 and 24 h), stained with Picro-Sirius Red. The imagens were captured with an inverted fluorescence microscope, Axiovert 200M (Zeiss, Germany). Under polarized light, Picro-Sirius Red staining marks the thick mature ColI fibers at pink-red, and thin immature fibers at blue-green. All images were taken at 10X magnification and scale bars correspond to 200 µm.

4.1.3 Chemical profile

ATR-FTIR analyses were performed to determine the chemical functional groups of Alg, ColI and Alg-ColI solutions (Fig. 4.6) and Alg and Alg-ColI hydrogels (Fig. 4.7). It should be noticed that hydrogels were freeze-dried in order to avoid the water absorption peaks in the analysis.

Alg solution displayed the typical Alg absorption bands [54-58], with the asymmetric and symmetric stretching of thw carboxylic group (−COO) on the polymeric backbone, found at 1599 and 1411 cm^{-1}, respectively (Fig. 4.6). It is also possible to identify bands corresponding to the hydroxyl group (−OH stretching) at 3326 cm^{-1} and the −CH stretching at 2933 cm^{-1}. The −CO group of the carboxyl is depicted at 1298 cm^{-1}, and the characteristic peak of mannuronic acid residues at 816 cm^{-1}. The peak observed at 1031 cm^{-1} occurred due to C−O−C antisymmetric stretching (Fig. 4.6).

In ColI0.125 solution, it was observed the characteristic Col absorption bands [41, 55, 57-59] corresponding to amide A (3307 cm^{-1}) and amide B (2927 and 2832 cm^{-1}) and the three main bands of the Col fingerprint: a) at 1601 cm^{-1} which relates to amide I due to carbonyl stretching −CH, b) at 1410 cm^{-1} which is typical of amide II due to vibrations of the N−H bond and C−N stretching and c) at 1298 cm^{-1} which corresponds to vibrations of amide III due to C−N stretching and N−H deformation (Fig. 4.6a-c). Similar results were found in the ATR-FTIR spectrum of ColI0.25 solution: the N-H stretching vibration peak for the amide A at 3305 cm^{-1}, and the N−H bond and C−N stretching peak for the amide B at 2926 and 2848 cm^{-1}. It is also possible to identify bands corresponding to amide I at 1599 cm^{-1}, amide II at 1409 cm^{-1}, and amide III at 1296 cm^{-1} (Fig. 4.6).

Alg-ColI solutions (Alg-ColI0.125 and Alg-ColI0.25) displayed Alg and ColI characteristics bands [57, 60], indicating a successful entrapment of ColI into the Alg matrix, without chemical reactions occurring between them (Fig. 4.6).

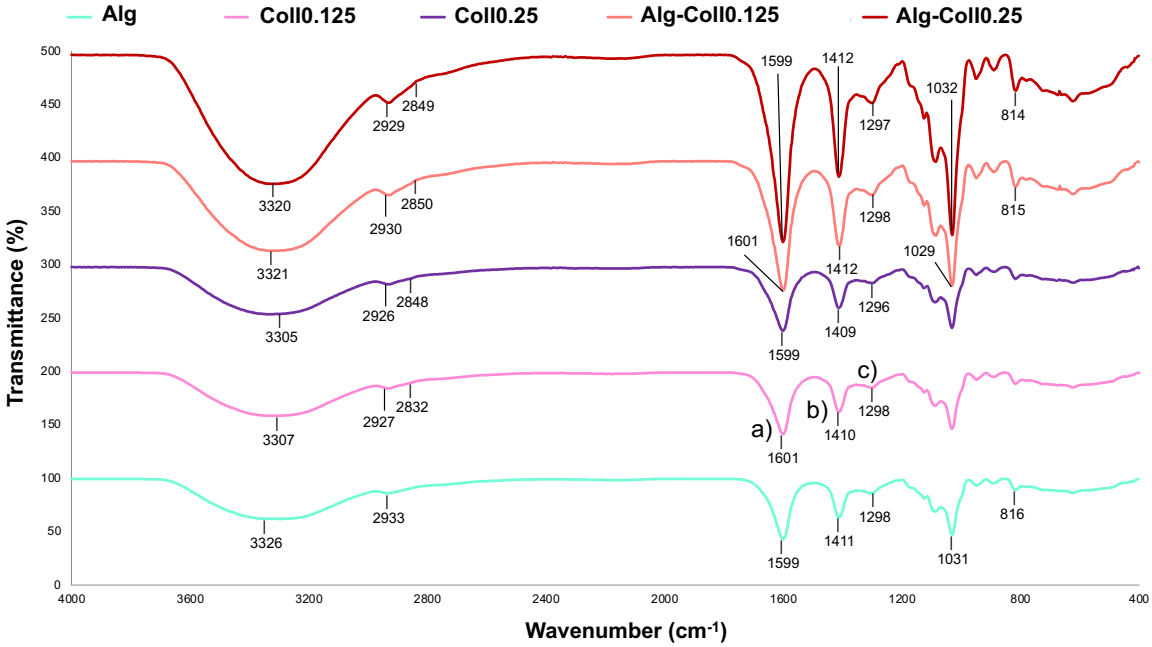

Figure 4.6 – ATR-FTIR spectra of the solutions of Alg, ColI and Alg-ColI solutions. (a-c) The three main bands of the Col fingerprint (Amide I, II and III).

Regarding ATR-FTIR spectra of Alg hydrogels, the typical absorption peaks of Alg [54-58] were detected in all conditions independent of temperature (RT and 37 ºC) and incubation time (0, 12 and 24 h) (Fig. 4.7). In detail, Alg hydrogel produced at RT (Fig.4.7a) showed characteristic peaks at 3322 cm^{-1} (−OH stretch), 2927 cm^{-1} (−CH stretch), 1593 and 1413 cm^{-1} (−COO asymmetric and symmetric stretch), 1292 cm^{-1} (−CO stretch), 1026 cm^{-1} (C−O−C antisymmetric stretch), and 816 cm^{-1} (−CO vibration of groups in mannuronic units). Whereas Alg hydrogel pre-incubated at 37 ºC for 24 h (Fig. 4.7b) displayed the absorption bands at 3318 cm^{-1} (−OH stretch), 2929 cm^{-1} (−CH stretch), 1591 and 1414 cm^{-1} (−COO asymmetric and symmetric stretch), 1292 cm^{-1} (−CO stretch), 1023 cm^{-1} (C−O−C antisymmetric stretch), and 817 cm^{-1} (−CO vibration of groups in mannuronic units). These results showed that temperature, incubation time and gelification process did not affect the chemical profile of Alg hydrogels.

Concerning ATR-FTIR spectra of Alg-ColI hydrogels, typical bands of Alg and ColI [57, 60] were detected on Alg-ColI0.125 and Alg-ColI0.25 hydrogels (Fig. 4.7 and Supplementary Material A), regardless the conditions used (temperature, incubation time and gelification process). In general, the ATR-FTIR spectrum of Alg-ColI hydrogels showed characteristic absorption bands at 3232 cm^{-1} corresponding to amide A and at 2924 and 2843 cm^{-1} corresponding to amide B bands. There is also observed a set of three bands at 1591, 1412 and 1291 cm^{-1} representing −CH stretch (Amide I), N−H bond plus C−N stretch (Amide II), and N−H deformation plus C−N stretch (Amide III), respectively. The absorption peaks at 1025 and 816 cm^{-1} presented in this spectrum occur due to C−O−C antisymmetric stretching vibration and −CO vibration of groups in mannuronic units of Alg, respectively (Fig. 4.7). From ATR-FTIR analyses, it is possible to conclude that ColI can be incorporated into the Alg network without altering its chemical structure, even using different conditions of hydrogel production.

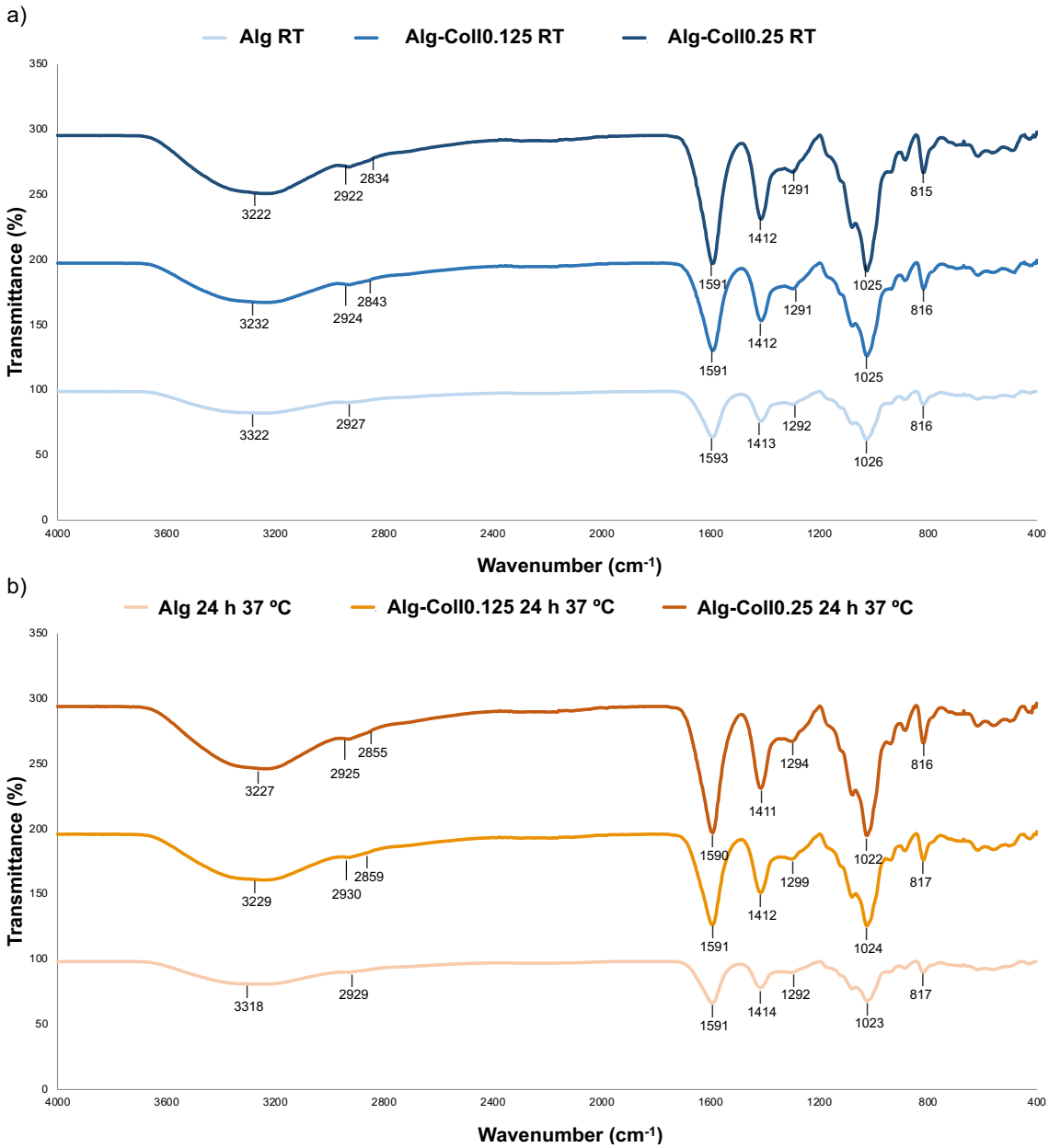

Figure 4.7 – ATR-FTIR spectra of of freeze-dried Alg and Alg-ColI samples at (a) RT and (b) incubated at 37 ºC for 24 h.

4.1.4 Swelling behavior and water content

The swelling behavior is an intrinsic property of hydrogels, where the gels enlarge due to solvent penetration into the space between the network chains [21]. Hydrogels can swell until the osmotic forces that help to extend the polymer network are balanced by the elastic forces from the stretched segments of the polymer, a phenomenon known as equilibrium [25, 27]. Moreover, they can retain large amounts of water or other aqueous solutions, an important condition for wound healing [61]. In this sense, the equilibrium swelling ratio and water content of produced hydrogels were evaluated, which is shown in Table 4.1. Comparing Alg (controls) and Alg-ColI hydrogels produced at RT, a reduction of swelling ratio and water content was observed in Alg-ColI hydrogels, indicating that the ColI incorporation could provide some resistance to water diffusion and swelling tendencies [47, 62]. However, when both hydrogels (Alg and Alg-ColI) were pre-incubated at 37 ºC for 12 and/or 24 h, the swelling ratio and water content of Alg-ColI hydrogels (Table 4.1) increased, probably, due to the hydrophilic properties of ColI [58, 60].

Alg hydrogels produced at RT and those pre-incubated at 37 ºC for 12 or 24 h showed differences significates in terms of swelling ratio and water content. The temperature and incubation time reduced the swelling ratio and water content of Alg hydrogels, i.e, decreased the Alg hydrogel's ability to swell and retain liquids (Table 4.1). While the Alg-ColI hydrogels pre-incubated at 37 ºC for 12 or 24 h showed a higher swelling ratio and water content compared to Alg-ColI hydrogels produced at RT (Table 4.1).

From all these results, it is possible to conclude that Alg-ColI0.25 hydrogels incubated at 37 ºC for 24 h may be useful for wound healing due to their high swelling ratio (ability for adsorbing the wound exudate) and water content (ability to maintain a physiologically moist environment) [46, 60, 62, 63].

Table 4.1 — The equilibrium swelling ratio and water content of Alg-ColI hydrogels.

Hydrogel	Temperature [°C]	Incubation time [h]	Swelling ratio [%]	Water Content [%]
Alg	RT	0	80.85 ± 0.97 %	97.46 ± 15.21 %
Alg-ColI0.125			79.60 ± 1.41 %$^{\#}$	97.32 ± 6.88 %
Alg-ColI0.25			77.73 ± 4.87 %$^{\#}$	97.08 ± 4.34 %$^{\#}$
Alg	37	12	57.25 ± 0.72 %*	97.29 ± 0.58 %*
Alg-ColI0.125			76.55 ± 0.62 %$^{\#}$	97.38 ± 0.91 %*,$^{\#}$
Alg-ColI0.25			78.34 ± 0.80 %$^{\#}$	97.35 ± 2.67 %*,$^{\#}$
Alg	37	24	62.76 ± 2.81 %*	97.17 ± 0.95 %*
Alg-ColI0.125			82.17 ± 0.10 %*,$^{\#}$	97.45 ± 1.38 %*,$^{\#}$
Alg-ColI0.25			82.58 ± 0.22 %$^{\#}$	97.47 ± 0.79 %*,$^{\#}$

Data were expressed as mean ± SD.
*Significant differences compared to hydrogel produced at RT (control), at same composition, with $p < 0.05$, obtained by Student's T-test.
$^{\#}$Significant differences compared to Alg (control) at same condition of production, with $p < 0.05$, obtained by Student's T-test.

4.1.5 Influence of pH on stability of the Alg-ColI hydrogels

As previously described (section 1.4), the human skin tissue is slightly acidic (around pH 5.5–6) [20], but after a certain injury (e.g., ionizing radiation), the pH of the wound increase to values in the alkaline range (around 8–8.5). In a functional healing process, the pH of the wound decreases gradually, from pH values in the alkaline range to the pH of intact skin. However, if the pH values remain at a high level, the healing process will slow down or even stop [20]. Since the pH varies throughout the healing process, this study evaluated the influence of pH values (5.5, 7.4 and 8.0) on the stability of Alg and Alg-ColI hydrogels (Fig. 4.8), to predict their behavior *in vivo* situation.

Regardless of their composition and production method, all hydrogels showed structural stability independently of pH values. But their physical behavior was dependent on pH value, i.e, at acid (5.5) pH the hydrogels shrank while at alkaline (8.0) pH occurred the puffing of their matrixes. Several authors [47, 64] have reported that this physical behavior is due to ionization and pronation of −COOH group on the Alg polysaccharide. So, under an alkaline solution the −COOH of the Alg is ionized, leading to swelling of Alg network. Contrarily, under acidic conditions occurs the protonation of the −COO groups of the Alg network, increasing the cross-linking degree of the network, and consequently promoting the shrinkage of the hydrogels [47, 65].

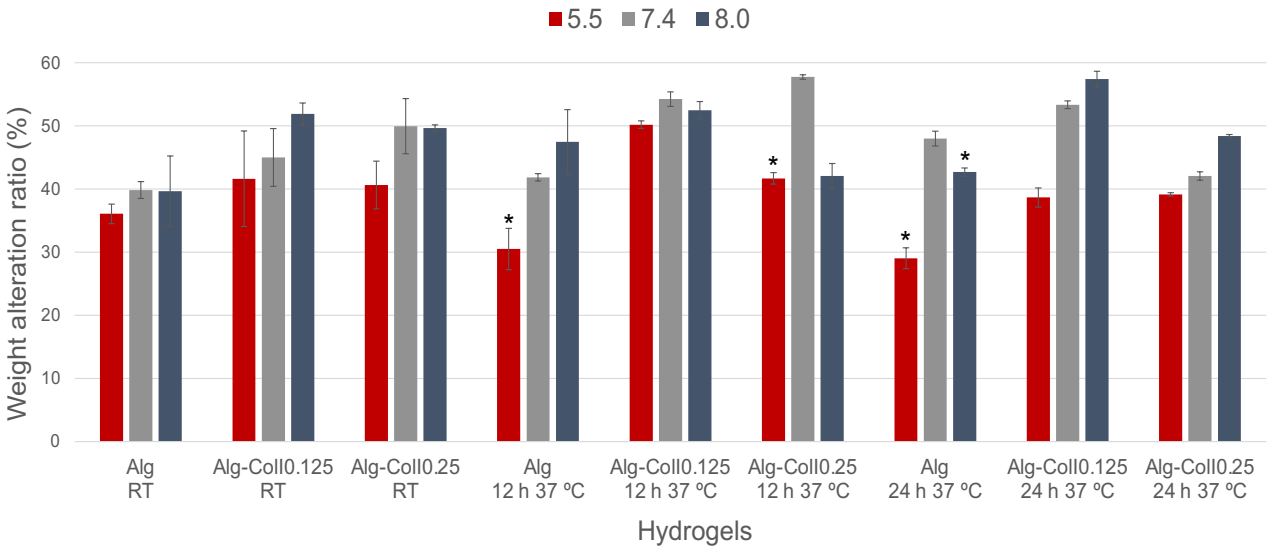

Figure 4.8 - Stability of the Alg and Alg-ColI hydrogels at different pH values (5.5, 7.4 and 8), after 3 h incubation. Data are expressed as mean ± SD (n = 6).
*Significant differences compared to pH 7.4 (control), for same hydrogel, with $p < 0.05$, obtained by Student's T-test.

4.1.6 Influence of proteins on stability of the Alg-ColI hydrogels

When a biomaterial contacts a biological tissue, one of the first events to occur is protein adsorption [65]. Thereby, this study evaluated if the adsorption of proteins could affect the stability of the Alg and Alg-ColI hydrogels. Figure 4.9 shows the weight alteration ratio of the

Alg and Alg-ColI hydrogels immersed in α-MEM with and without FBS, after 1 (figure 4.9a) and 7 days (figure 4.9b).

Regarding the 1st day results, no significant differences were shown between hydrogels immersed in α-MEM with and without FBS, i.e., the adsorption of proteins did not influence the weight of the hydrogels (Figure 4.9a). Contrarily, after 7 days of incubation, there were significant differences between the hydrogels immersed in α-MEM with and without FBS (Figure 4.9b). In this case, the presence of proteins in media led to increasing the weight of hydrogels, but without the breakdown of their matrixes, indicating that Alg-ColI hydrogels are capable of adsorbing proteins while maintaining their integrity.

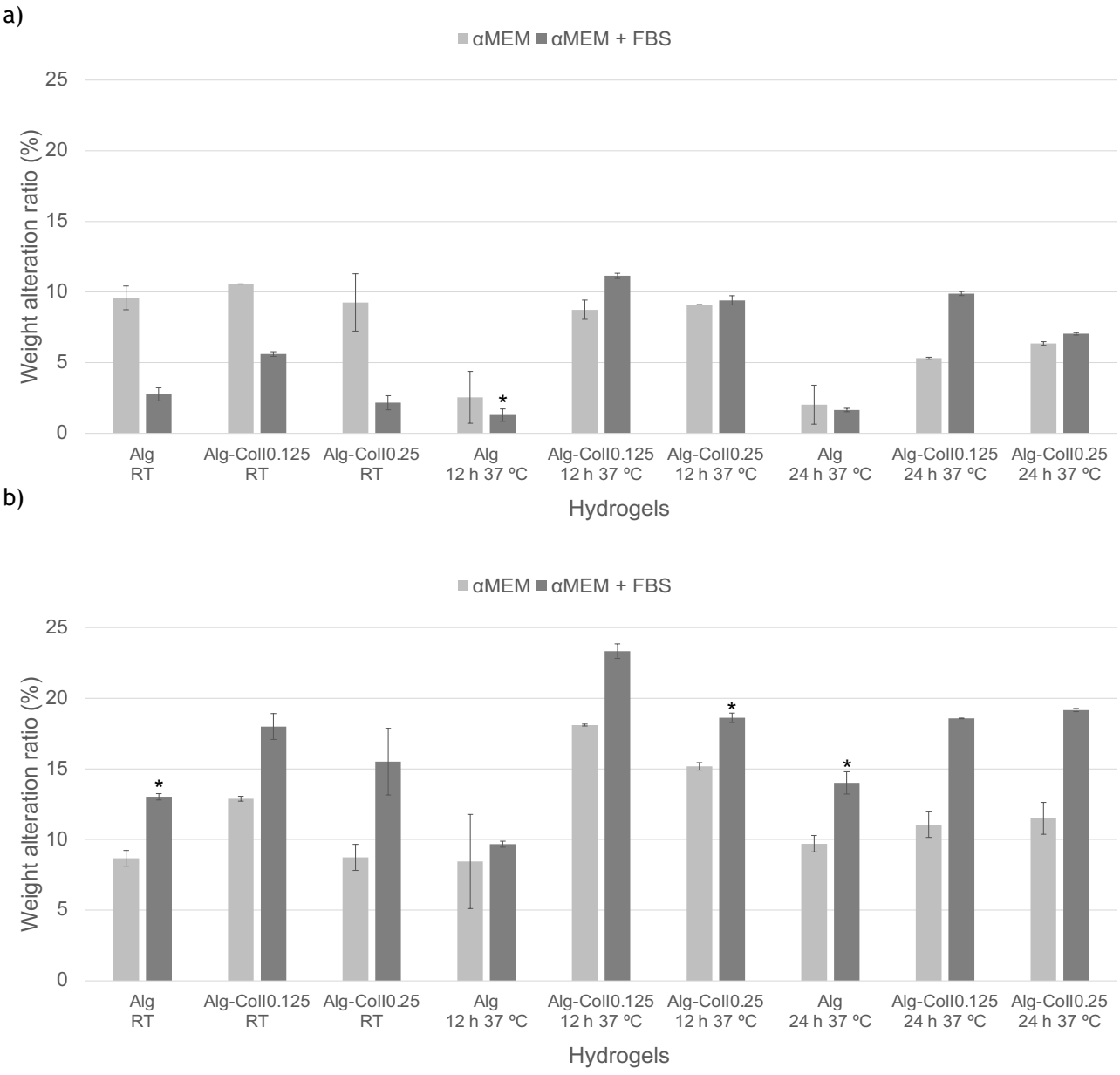

Figure 4.9 - Stability of the Alg and Alg-ColI hydrogels in α-MEM with and without FBS (control), after (a) 1 and (b) 7 days of incubation at 37 ºC. Data are expressed as mean ± SD (n = 3).
*Significant differences compared to control (α-MEM without FBS), at same hydrogel, with $p < 0.05$, obtained by Student's T-test.

4.2 Cell Culture

4.2.1 *In vitro* cytocompatibility of Alg-ColI hydrogels

Cell metabolic activity can provide relevant information about the capability of cells to grow and proliferate in the presence of biomaterials [66, 67]. Figure 4.10 is shown the HDF cells' growth (metabolic activity) in presence of Alg and Alg-ColI hydrogels for 24 and 72 h. The cell metabolic activity was reduced in the presence of both hydrogels, contributing to a decrease in cell growth rate compared to control (HDF cells without hydrogels). However, the cells in the presence of hydrogels continued to grow throughout the culture time, being observed with a significant increase in metabolic activity from 24 to 72 h for all samples (Fig. 4.10). Besides, it was observed that at 72 h of culture, similar cell metabolic activity was observed between Alg-ColI0.25 hydrogels prepared at RT, Alg hydrogels pre-incubated at 37 ºC for 12 and control (Fig. 4.10). Moreover, some hydrogels (Alg at RT, Alg-ColI0.125 at RT, and Alg-ColI pre-incubated at 37 ºC for 12 h) showed much close cell metabolic activity to the control at 72 h of culture. These data suggest that hydrogels did not affect the cell viability, since the cells continued to grow and proliferate but at a slower rate compared to the control. Similar results were found in a study performed by Rehman et al, where the authors showed that after 1 day in culture, the cell metabolic activity was reduced in the presence of 0.004 wt % rGO loaded GelMA hydrogel, being observed an increasing of metabolic activity from 1 to 3 days in culture [66]. Rehman et al, [66] also showed that the proliferation of fibroblasts cells exposed to GelMA hydrogels significantly increased after 5 days in culture as compared to 1 and 3 days.

Regarding the cell growth in the presence of Alg hydrogels and Alg-ColI, no significant differences were found between them (Fig. 4.10), suggesting that the incorporation of ColI on Alg matrix did not show a cytotoxic effect, even using high ColI concentrations (ColI0.25 %). These data are in accordance with a study performed by Tierney et al, where the authors showed that three different Col contents (0.25 %, 0.5 % and 1 %) did not affect the cellular number or metabolic activity [68].

Comparing the cell metabolic activity in the presence of hydrogels produced at RT and at 37 ºC for 12/24 h, no differences were observed between them (Fig. 4.10), indicating that the temperature (RT and 37 ºC) and incubation time (0, 12 and 24 h) used to produce hydrogels did not affect the cell growth. Moxon et at, showed that the incubation of Alg-Col solutions at 37 °C for 4 h, prior to gelification, did not affect the proliferation and migration of encapsulated human iPSC-derived neurons [49].

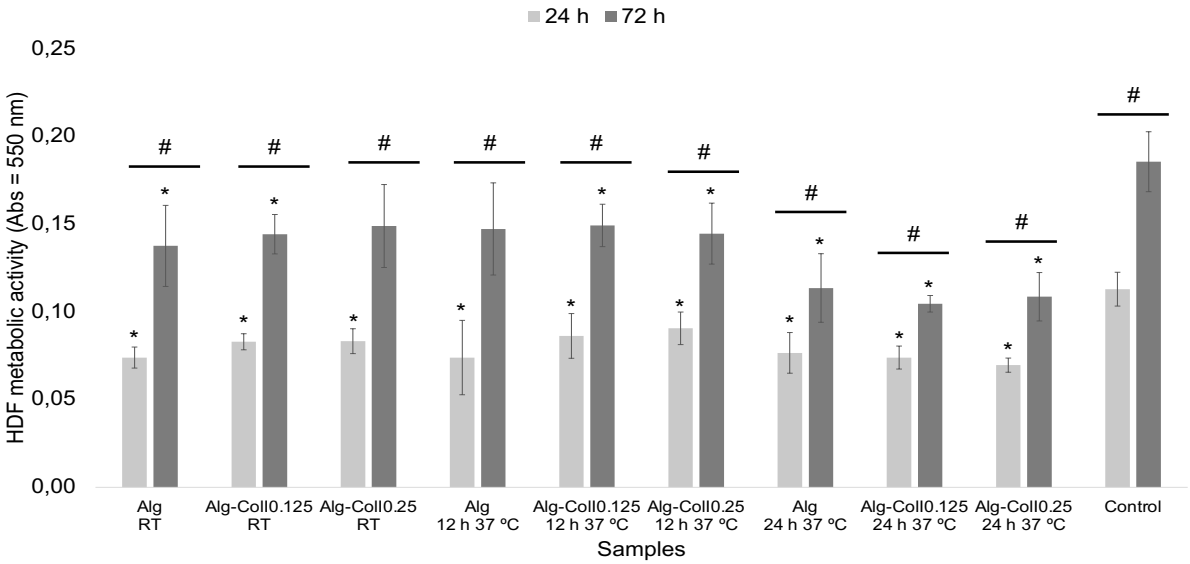

Figure 4.10 – Metabolic activity of HDF cells exposed to the Alg and Alg-ColI hydrogels for periods of 24 and 72 h. Cells cultured in the absence of the hydrogels were used as control. Data were expressed as mean ± SD (n = 3).
*Significant differences compared to control (without material), at same time-point, with $p < 0.05$, obtained by Student's T-test. #Significant differences between time-points (24 compared to 72 h), at same hydrogel, with $p < 0.05$, obtained by Student's T-test.

4.2.2 Influence of radiation in metabolic activity and cell proliferation

The effect of ionizing radiation in HDF cells after 24 h culture is shown in Figure 4.11. It should be noticed that non-irradiated HDF cells were equally manipulated as irradiated HDF cells, but they were not exposed to ionizing radiation.

No significant differences in cell metabolic activity were observed between non-irradiated and irradiated cells, however, there seems to be a tendency toward higher values in irradiated cells as compared to non-irradiated. This slight increase in metabolic activity values seems to be related to the increase of cell proliferation after irradiation [67]. It has been reported for many years [69, 70] that when cells are exposed to low doses of ionizing radiation (e.g., 1-2 Gy), the probability of immediate DNA damage is extremely small. In this case, ionizing radiation led to an increase of apoptosis of damaged cells followed by cell proliferation [70]. Furthermore, Acharya et al, [71] reported that cells surviving irradiation upregulate their metabolic state to compensate for the damage incurred during exposure. Therefore, these results (Fig. 4.11) are consistent with the literature, as it is possible to observe a slight increase in cell proliferation in HDF cells that were irradiated with 2 Gy compared to HDF cells that were not irradiated, 24 h after incubation.

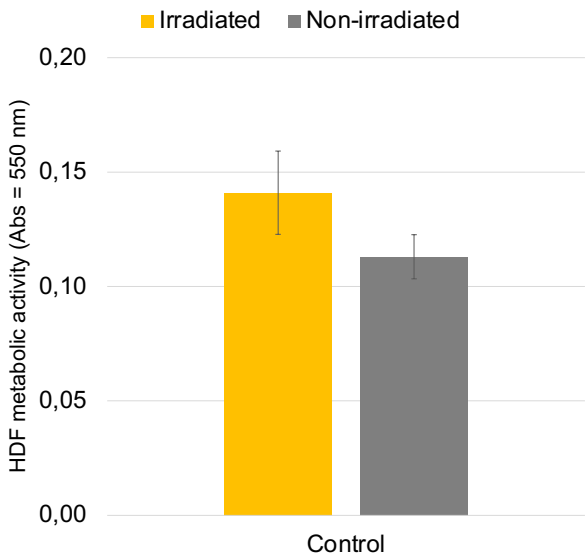

Figure 4.11 – Metabolic activity of irradiated and non-irradiated HDF cells after 24 h of incubation. HDF cells cultured in the absence of the hydrogels were used as control. Data were expressed as mean ± SD (n = 3).

4.2.3 Regenerative effect of Alg-ColI hydrogels on irradiated cells

Figure 4.12 shows the metabolic activity of irradiated HDF cells in the presence of the Alg and Alg-ColI hydrogels for periods of 24 and 72 h.

Once again it was found that the irradiated cell metabolic activity was lower in the presence of hydrogels compared to control over the 72 h of culture (Fig. 4.12). Contrarily to non-irradiated cells, here, no differences in irradiated cells growth were found between 24 and 72 h of incubation, regardless of hydrogel used (Fig. 4.12).

Although ionizing radiation caused an initial increase in cell proliferation (Fig. 4.11), 72 h after exposure (figure 4.12) the HDF cells maintained similar values of metabolic activity, which is not in agreement with what was observed in the non-irradiated cells (Fig. 4.10). This means that ionizing radiation slows down cell growth, independently of the presence or absence of the hydrogel.

The potential regenerative effect of Alg-ColI hydrogels would be observed if there was an increase in the expression of cell metabolic activity compared to control (without hydrogel) [72]. Eventually, longer culture times after radiation exposure would contribute to selecting the hydrogel with an effective regenerative effect.

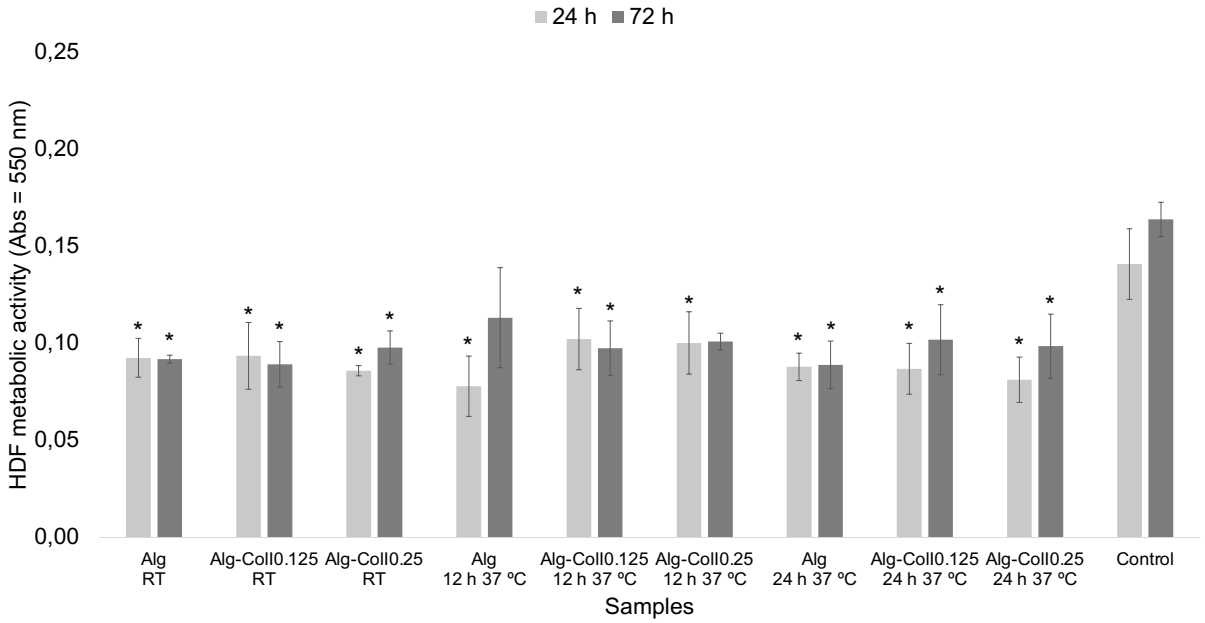

Figure 4.12 – Metabolic activity of irradiated HDF cells exposed to the Alg and Alg-ColI hydrogels for periods of 24 and 72 h. Irradiated cells cultured in the absence of the hydrogels were used as controls. Data were expressed as mean ± SD (n = 3).

4.2.4 Immunofluorescence analysis of irradiated cells

Figure 4.13 shows the organization and morphology of irradiated HDF cells exposed to Alg and Alg-ColI hydrogels over 24 h of culture. Control samples (irradiated HDF cells not exposed to hydrogels) showed typical fibroblasts morphology [47, 73, 74], namely a dense network of F-actin filaments organized as stress fibers, with cells presenting an elongated and flattened morphology. It is also possible to observe abundant cell-to-cell contact. Identical appearance and morphology were observed in irradiated HDF cells in the present of Alg and Alg-ColI hydrogels, and no morphological and organizational differences were found between hydrogels used (Fig. 4.13).

Fibroblasts are essential to the wound healing process as they deposit a temporary tissue matrix allowing the skin to recover from injury [16]. Their morphology and cytoskeletal organization are important for cell homeostasis [47]. Notably, fibroblasts contain a cytoskeletal protein named actin, and its distribution in fibroblast cells is very important for wound healing [75]. As can be seen (Fig. 4.13) the cytoskeleton F-actin organization, nucleus, and morphology of irradiated HDF cells in the absence (control) of hydrogels are similar to those exposed to hydrogels. This means Alg-ColI hydrogels do not change the cytoskeleton F-actin organization and cell morphology.

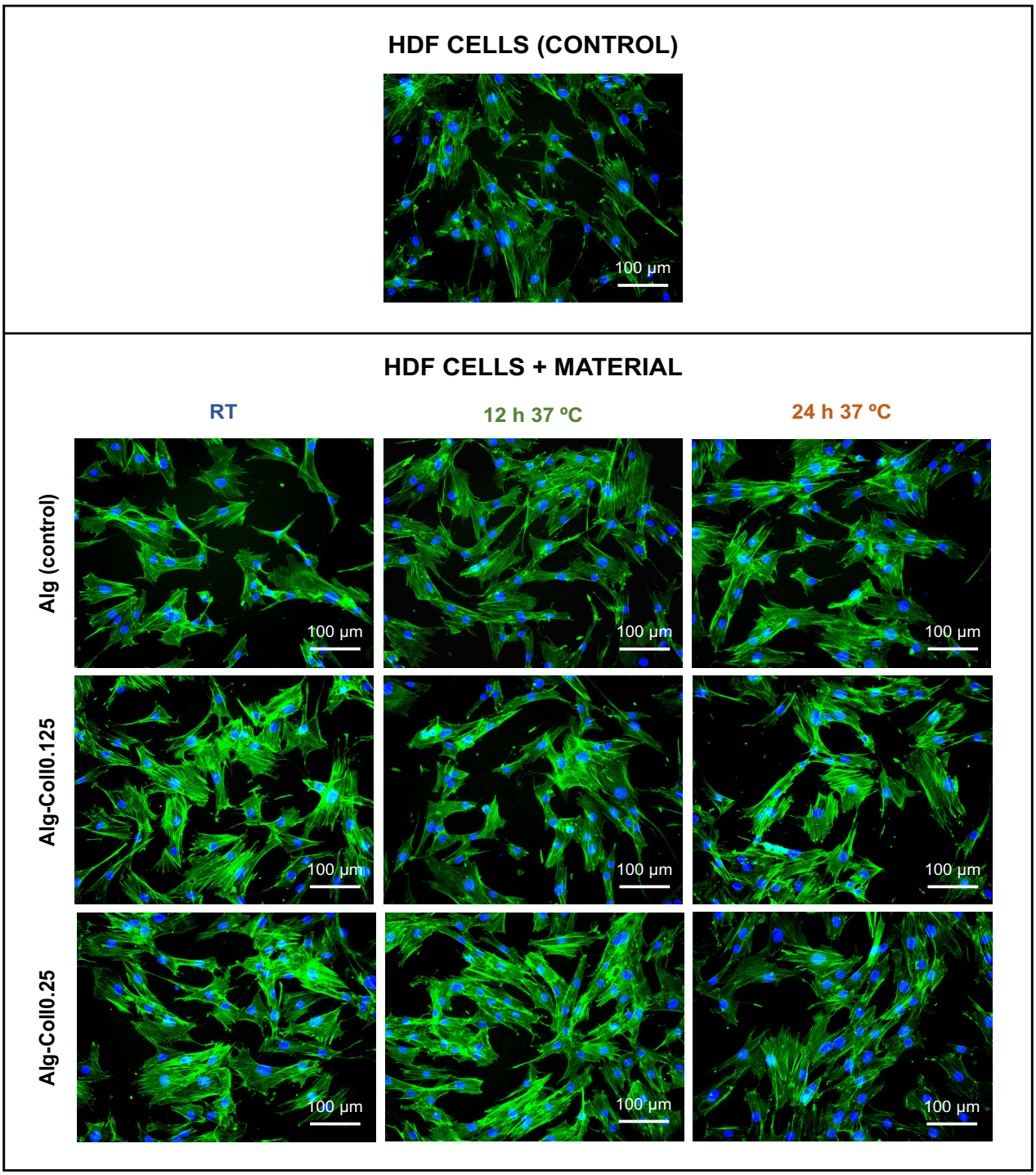

Figure 4.13 – Immunofluorescent images of irradiated HDF cells in the absence (control) and presence of Alg and Alg-Coll hydrogels, after 24 h of irradiation. Cell cytoskeleton F-actin was stained green and nucleus counterstained in blue. Scale bar corresponds to 100 µm.

Chapter 5

Conclusion

Radiotherapy plays an important role in cancer treatment. However, this therapeutic modality can cause a skin lesion known as radiodermatitis. This common side effect of radiotherapy particularly affects the quality of life of patients. In the last years, some therapeutic approaches have been developed to improve the wound healing process, but the treatment of radiodermatitis still remains a challenge. Among the different wound dressings developed so far, hydrogels are one of the possibilities with great potential to mimic the native skin microenvironment. In fact, hydrogels can absorb wound exudate maintaining a physiologically moist environment for the healing process.

In this study, Alg-ColI hydrogels were developed and characterized in terms of morphology, chemical composition, swelling behavior, water content, pH-responsive behavior, and protein adsorption. Additionally, human dermal fibroblasts under and without radiation treatment were cultured to assess the *in vitro* cytocompatibility and regenerative effect of the hydrogels.

The morphology of hydrogels was characterized by SEM and TEM analyses and showed that temperature (37 ºC), incubation time (12 and 24 h) and ColI concentration (0.25 %) appear to induce an increase of ColI fibrils formation which could be important to promote cell adhesion and proliferation. Histochemical analysis of hydrogels allowed to confirm the formation and maturation of ColI fibrils in the Alg network.

From FTIR, was concluded that ColI can be incorporated into Alg network without altering their chemical structure, even using different conditions of hydrogel production.

Regarding the swelling behavior and water content, the hydrogels showed a great ability to absorb exudate maintaining a physiologically moist environment. Addditionally, they showed to be stable at different pH values (5.5, 7.4, and 8.0) and capable of adsorbing proteins while maintaining their integrity.

The Alg-ColI hydrogels showed to be cytocompatible, allowing the cell growth and proliferate from 24 to 72 h of culture. The potential regenerative effect of Alg-ColI hydrogels was not possible to observe due to the used culture times (72 h). However, the hydrogels showed good biocompatibility, once the irradiated cells grew in the presence of Alg-ColI hydrogels with similar cell morphology and cytoskeletal organization (actin) compared to the control (without hydrogel), which is an important feature for wound healing.

In summary, the Alg-ColI hydrogels showed promising properties in terms of maintaining a healthy physiological milieu and promoting cell proliferation even after radiotherapy. Thereby,

the Alg-ColI hydrogels seem to have promising properties for the wound healing process and consequently radiodermatitis treatment.

Chapter 6

Future Perspectives

Although this project is still in a very early stage, the truth is that the work presented very promising results, and therefore more studies should be done.

In the short-term, for instance, *in vitro* biodegradation tests should be conducted to determine the biodegradability of Alg and Alg-ColI hydrogels. Also, the regenerative effect of Alg and Alg-ColI hydrogels should be evaluated using longer cultures times.

In the long-term, it will be necessary for a better understanding of the biological process resulting from skin exposure to ionizing radiation and produced hydrogels. The cellular mechanisms involved both during radiodermatitis and in its healing process should be also studied, as well as gene expression analysis.

References

[1] C. Mattiuzzi and G. Lippi, "Current Cancer Epidemiology," J Epidemiol Glob Health, vol. 9, no. 4, pp. 217-222, Dec 2019, doi: 10.2991/jegh.k.191008.001.

[2] J. Skliarenko and A. Barry, "Clinical and practical applications of radiation therapy: when should radiation therapy be considered for my patient?," Medicine, vol. 48, no. 2, pp. 84-89, 2020/02/01/ 2020, doi: https://doi.org/10.1016/j.mpmed.2019.11.004.

[3] K. K. Fu, T. F. Pajak, A. Trotti, C. U. Jones, S. A. Spencer, T. L. Phillips, A. S. Garden, J. A. Ridge, J. S. Cooper, K. K. Ang, and Grp. Radiation Therapy Oncology, "A Radiation Therapy Oncology Group (RTOG) phase III randomized study to compare hyperfractionation and two variants of accelerated fractionation to standard fractionation radiotherapy for head and neck squamous cell carcinomas: First report of RTOG 9003," (in English), Int J Radiat Oncol, vol. 48, no. 1, pp. 7-16, Aug 1 2000, doi: Doi 10.1016/S0360-3016(00)00663-5.

[4] A. Elgazzar and N. Kazem, "Biological Effects of Ionizing Radiation," The Pathophysiologic Basis of Nuclear Medicine: Second Edition, pp. 715-726, 06/01 2015, doi: 10.1007/978-3-319-06112-2_21.

[5] J. Robijns and H.-J. Laubach, "Acute and chronic radiodermatitis: clinical signs, pathophysiology, risk factors and management options," Journal of the Egyptian Women's Dermatologic Society, vol. 15, no. 1, 2018.

[6] F. N. Bray, B. J. Simmons, A. H. Wolfson, and K. Nouri, "Acute and Chronic Cutaneous Reactions to Ionizing Radiation Therapy," (in English), Dermatology Ther, vol. 6, no. 2, pp. 185-206, Jun 2016, doi: 10.1007/s13555-016-0120-y.

[7] F. Hegedus, L. M. Mathew, and R. A. Schwartz, "Radiation dermatitis: an overview," (in eng), Int J Dermatol, vol. 56, no. 9, pp. 909-914, Sep 2017, doi: 10.1111/ijd.13371.

[8] M. Singh, A. Alavi, R. Wong, and S. Akita, "Radiodermatitis: A Review of Our Current Understanding," (in eng), Am J Clin Dermatol, vol. 17, no. 3, pp. 277-92, Jun 2016, doi: 10.1007/s40257-016-0186-4.

[9] S. Seité, R.-J. Bensadoun, and J.-M. Mazer, "Prevention and treatment of acute and chronic radiodermatitis," (in eng), Breast Cancer (Dove Med Press), vol. 9, pp. 551-557, 2017, doi: 10.2147/BCTT.S149752.

[10] C. B. V. de Andrade, I. P. R. Ramos, A. C. N. de Moraes, A. L. R. do Nascimento, C. Salata, R. Goldenberg, J. J. de Carvalho, and C. E. V. de Almeida, "Radiotherapy-Induced Skin Reactions Induce Fibrosis Mediated by TGF-ß1 Cytokine," (in eng), Dose Response, vol. 15, no. 2, p. 1559325817705019, Apr-Jun 2017, doi: 10.1177/1559325817705019.

[11] J. D. Cox, J. Stetz, and T. F. Pajak, "Toxicity Criteria of the Radiation-Therapy Oncology Group (Rtog) and the European-Organization-for-Research-and-Treatment-of-Cancer (Eortc)," (in English), Int J Radiat Oncol, vol. 31, no. 5, pp. 1341-1346, Mar 30 1995, doi: Doi 10.1016/0360-3016(95)00060-C.

[12] S. Zenda, Y. Ota, H. Tachibana, H. Ogawa, S. Ishii, C. Hashiguchi, T. Akimoto, Y. Ohe, and Y. Uchitomi, "A prospective picture collection study for a grading atlas of radiation

dermatitis for clinical trials in head-and-neck cancer patients," (in eng), J Radiat Res, vol. 57, no. 3, pp. 301-6, Jun 2016, doi: 10.1093/jrr/rrv092.

[13] K. C. Turke, J. H. M. Schoueri, A. V. C. Oliveira, V. Lippi, F. R. Lobo, J. G. Fraga, C. Campos, V. Salzano, C. Machado, A. del Giglio, and D. G. Fabra, "Management and Treatment of Radiodermatitis in Cancer Patients: Case Series," Clinical Oncology Letters, 2020. [Online]. Available: https://www.clinicaloncologyletters.com/article/10.4322/col.2019.006/pdf/col-0-AheadOfPrint-5f1095e70e8825ca215a5968.pdf

[14] S. A. Mohamed and R. Hargest, "Surgical anatomy of the skin," Surgery (Oxford), vol. 40, no. 1, pp. 1-7, 2022/01/01/ 2022, doi: https://doi.org/10.1016/j.mpsur.2021.11.021.

[15] R. Wong, S. Geyer, W. Weninger, J. C. Guimberteau, and J. K. Wong, "The dynamic anatomy and patterning of skin," (in eng), Exp Dermatol, vol. 25, no. 2, pp. 92-8, Feb 2016, doi: 10.1111/exd.12832.

[16] K. Vig, A. Chaudhari, S. Tripathi, S. Dixit, R. Sahu, S. Pillai, V. A. Dennis, and S. R. Singh, "Advances in Skin Regeneration Using Tissue Engineering," (in eng), Int J Mol Sci, vol. 18, no. 4, Apr 7 2017, doi: 10.3390/ijms18040789.

[17] P. Juhl, A.-C. Bay-Jensen, M. Karsdal, A. S. Siebuhr, N. Franchimont, and J. Chavez, "Serum biomarkers of collagen turnover as potential diagnostic tools in diffuse systemic sclerosis: A cross-sectional study," PLOS ONE, vol. 13, no. 12, p. e0207324, 2018, doi: 10.1371/journal.pone.0207324.

[18] S. Tavakoli and A. S. Klar, "Advanced Hydrogels as Wound Dressings," (in eng), Biomolecules, vol. 10, no. 8, p. 1169, 2020, doi: 10.3390/biom10081169.

[19] C. Shi, C. Wang, H. Liu, Q. Li, R. Li, Y. Zhang, Y. Liu, Y. Shao and J. Wang, "Selection of Appropriate Wound Dressing for Various Wounds," (in eng), Front Bioeng Biotechnol, vol. 8, pp. 182-182, 2020, doi: 10.3389/fbioe.2020.00182.

[20] S. Auerswald, S. Schreml, R. Meier, A. Blancke Soares, M. Niyazi, S. Marschner, C. Belka, M. Canis, and F. Haubner, "Wound monitoring of pH and oxygen in patients after radiation therapy," Radiat Oncol, vol. 14, no. 1, p. 199, Nov 11 2019, doi: 10.1186/s13014-019-1413-y.

[21] M. Bahram, N. Mohseni, and M. Moghtader, "An Introduction to Hydrogels and Some Recent Applications," in Emerging Concepts in Analysis and Applications of Hydrogels, 2016, ch. 2.

[22] S. Mantha, S. Pillai, P. Khayambashi, A. Upadhyay, Y. Zhang, O. Tao, H. M. Pham and S. D. Tran, "Smart Hydrogels in Tissue Engineering and Regenerative Medicine," (in eng), Materials (Basel, Switzerland), vol. 12, no. 20, p. 3323, 2019, doi: 10.3390/ma12203323.

[23] L. C. Hsu, B. Y. Peng, M. S. Chen, B. Thalib, M. Ruslin, T. D. X. Tung, H-H Chou, and K-L Ou, "The potential of the stem cells composite hydrogel wound dressings for promoting wound healing and skin regeneration: In vitro and in vivo evaluation," (in eng), J Biomed Mater Res B Appl Biomater, vol. 107, no. 2, pp. 278-285, Feb 2019, doi: 10.1002/jbm.b.34118.

[24] I. Negut, G. Dorcioman, and V. Grumezescu, "Scaffolds for Wound Healing Applications," (in eng), Polymers, vol. 12, no. 9, p. 2010, 2020, doi: 10.3390/polym12092010.

[25] M. Rizwan, R. Yahya, A. Hassan, M. Yar, A. D. Azzahari, V. Selvanathan, F. Sonsudin and C. N. Abouloula, "pH Sensitive Hydrogels in Drug Delivery: Brief History, Properties, Swelling, and Release Mechanism, Material Selection and Applications," (in eng), Polymers, vol. 9, no. 4, p. 137, 2017, doi: 10.3390/polym9040137.

[26] M. Beaumont, R. Tran, G. Vera, D. Niedrist, A. Rousset, R. Pierre, V. P. Shastri, and A. Forget, "Hydrogel-Forming Algae Polysaccharides: From Seaweed to Biomedical Applications," (in English), Biomacromolecules, vol. 22, no. 3, pp. 1027-1052, Mar 2021, doi: 10.1021/acs.biomac.0c01406.

[27] A. H. Karoyo and L. D. Wilson, "A Review on the Design and Hydration Properties of Natural Polymer-Based Hydrogels," (in eng), Materials (Basel), vol. 14, no. 5, Feb 26 2021, doi: 10.3390/ma14051095.

[28] S. Dhivya, V. V. Padma, and E. Santhini, "Wound dressings - a review," (in English), Biomedicine-Taiwan, vol. 5, no. 4, pp. 24-28, Dec 2015, doi: 10.7603/s40681-015-0022-9.

[29] H. Geckil, F. Xu, X. H. Zhang, S. Moon, and U. Demirci, "Engineering hydrogels as extracellular matrix mimics," (in English), Nanomedicine-Uk, vol. 5, no. 3, pp. 469-484, Apr 2010, doi: 10.2217/Nnm.10.12.

[30] W. Aljohani, L. Wenchao, M. Ullah, X. Zhang, and G. Yang, "Application of Sodium Alginate Hydrogel," IOSR Journal of Biotechnology and Biochemistry, vol. 03, pp. 19-31, 05/01 2017, doi: 10.9790/264X-03031931.

[31] B. A. Aderibigbe and B. Buyana, "Alginate in Wound Dressings," Pharmaceutics, vol. 10, no. 2, Apr 2 2018, doi: 10.3390/pharmaceutics10020042.

[32] T. Ramdhan, S. H. Ching, S. Prakash, and B. Bhandari, "Time dependent gelling properties of cuboid alginate gels made by external gelation method: Effects of alginate-CaCl2 solution ratios and pH," Food Hydrocolloids, vol. 90, pp. 232-240, 2019/05/01/ 2019, doi: https://doi.org/10.1016/j.foodhyd.2018.12.022.

[33] G. Kaklamani, D. Cheneler, L. M. Grover, M. J. Adams, and J. Bowen, "Mechanical properties of alginate hydrogels manufactured using external gelation," Journal of the Mechanical Behavior of Biomedical Materials, vol. 36, pp. 135-142, 2014/08/01/ 2014, doi: https://doi.org/10.1016/j.jmbbm.2014.04.013.

[34] H. Yan, D. Huang, X. Chen, H. Liu, Y. Feng, Z. Zhao, Z Dai, X. Zhang, and Q. Lin, "A novel and homogeneous scaffold material: preparation and evaluation of alginate/bacterial cellulose nanocrystals/collagen composite hydrogel for tissue engineering," Polymer Bulletin, vol. 75, pp. 1-16, 03/01 2018, doi: 10.1007/s00289-017-2077-0.

[35] J. Venkatesan, R. Jayakumar, S. Anil, E. Chalisserry, R. Pallela, and S.-K. Kim, "Development of Alginate-Chitosan-Collagen Based Hydrogels for Tissue Engineering," Journal of Biomaterials and Tissue Engineering, vol. 5, pp. 458-464, 09/01 2015, doi: 10.1166/jbt.2015.1338.

[36] B. Palma Santana, F. Nedel, E. Piva, R. Varella de Carvalho, F. Fernando Demarco, and N. Lenin Villarreal Carreño, "Preparation, Modification, and Characterization of Alginate Hydrogel with Nano-/Microfibers: A New Perspective for Tissue Engineering," BioMed Research International, vol. 2013, p. 307602, 2013/06/05 2013, doi: 10.1155/2013/307602.

[37] J. P. Paques, "Chapter 3 - Alginate Nanospheres Prepared by Internal or External Gelation with Nanoparticles," in Microencapsulation and Microspheres for Food Applications, L. M. C. Sagis Ed. San Diego: Academic Press, 2015, pp. 39-55.

[38] P. E. Ramos, P. Silva, M. M. Alario, L. M. Pastrana, J. A. Teixeira, M. A. Cerqueira, and A. A. Vicente, "Effect of alginate molecular weight and M/G ratio in beads properties foreseeing the protection of probiotics," Food Hydrocolloids, vol. 77, pp. 8-16, 2018/04/01/ 2018, doi: https://doi.org/10.1016/j.foodhyd.2017.08.031.

[39] M. Baniasadi and M. Minary-Jolandan, "Alginate-Collagen Fibril Composite Hydrogel," (in English), Materials, vol. 8, no. 2, pp. 799-814, Feb 2015, doi: 10.3390/ma8020799.

[40] A. Sorushanova, L. M. Delgado, Z. Wu, N. Shologu, A. Kshirsagar, R. Raghunath and D. I. Zeugolis, "The Collagen Suprafamily: From Biosynthesis to Advanced Biomaterial Development," (in eng), Adv Mater, vol. 31, no. 1, p. e1801651, Jan 2019, doi: 10.1002/adma.201801651.

[41] T. Riaz, R. Zeeshan, F. Zarif, K. Ilyas, N. Muhammad, S. Z. Safi, A. Rahim, S. A. A. Rizvi and I. U. Rehman, "FTIR analysis of natural and synthetic collagen," Applied

Spectroscopy Reviews, vol. 53, no. 9, pp. 703-746, 2018/10/21 2018, doi: 10.1080/05704928.2018.1426595.

[42] K. Lin, D. Zhang, M. H. Macedo, W. Cui, B. Sarmento, and G. Shen, "Advanced Collagen-Based Biomaterials for Regenerative Biomedicine," Advanced Functional Materials, vol. 29, no. 3, p. 1804943, 2019, doi: https://doi.org/10.1002/adfm.201804943.

[43] T. Hu and A. C. Y. Lo, "Collagen–Alginate Composite Hydrogel: Application in Tissue Engineering and Biomedical Sciences," Polymers, vol. 13, no. 11, p. 1852, 2021. [Online]. Available: https://www.mdpi.com/2073-4360/13/11/1852.

[44] S. Bierbaum, "Artificial Extracellular Matrices to Functionalize Biomaterial Surfaces," 2017, vol. 2: Comprehensive Biomaterials II, doi: 10.1016/B978-0-12-803581-8.10206-1.

[45] M. Meyer, "Processing of collagen based biomaterials and the resulting materials properties," BioMedical Engineering OnLine, vol. 18, no. 1, p. 24, 2019/03/18 2019, doi: 10.1186/s12938-019-0647-0.

[46] S. S. Mathew-Steiner, S. Roy, and C. K. Sen, "Collagen in Wound Healing," (in eng), Bioengineering (Basel), vol. 8, no. 5, p. 63, 2021, doi: 10.3390/bioengineering8050063.

[47] J. Barros, M. P. Ferraz, J. Azeredo, M. H. Fernandes, P. S. Gomes, and F. J. Monteiro, "Alginate-nanohydroxyapatite hydrogel system: Optimizing the formulation for enhanced bone regeneration," Mater Sci Eng C Mater Biol Appl, vol. 105, p. 109985, Dec 2019, doi: 10.1016/j.msec.2019.109985.

[48] S. Miranda, M. Correia, A. G. Dias, A. Pestana, P. Soares, J. Nunes, J. Lima, V. Maximo, and P. Boaventura, "Evaluation of the role of mitochondria in the non-targeted effects of ionizing radiation using cybrid cellular models," Sci Rep, vol. 10, no. 1, p. 6131, Apr 9 2020, doi: 10.1038/s41598-020-63011-w.

[49] S. R. Moxon, N. J. Corbett, K. Fisher, G. Potjewyd, M. Domingos, and N. M. Hooper, "Blended alginate/collagen hydrogels promote neurogenesis and neuronal maturation," Materials Science and Engineering: C, vol. 104, p. 109904, 2019/11/01/ 2019, doi: https://doi.org/10.1016/j.msec.2019.109904.

[50] N. Zerbinati and A. Calligaro, "Calcium hydroxylapatite treatment of human skin: evidence of collagen turnover through picrosirius red staining and circularly polarized microscopy," (in eng), Clin Cosmet Investig Dermatol, vol. 11, pp. 29-35, 2018, doi: 10.2147/ccid.S143015.

[51] O. Ovchinnikova, A. K. Robertson, D. Wagsater, E. J. Folco, M. Hyry, J. Myllyharju, P. Eriksson, P. Libby, G. K. Hansson, "T-cell activation leads to reduced collagen maturation in atherosclerotic plaques of Apoe(-/-) mice," Am J Pathol, vol. 174, no. 2, pp. 693-700, Feb 2009, doi: 10.2353/ajpath.2009.080561.

[52] R. E. Rivero, V. Capella, A. Cecilia Liaudat, P. Bosch, C. A. Barbero, N. Rodriguez, and C. R. Rivarola, "Mechanical and physicochemical behavior of a 3D hydrogel scaffold during cell growth and proliferation," RSC Adv, vol. 10, no. 10, pp. 5827-5837, Feb 4 2020, doi: 10.1039/c9ra08162c.

[53] J. Liu, M. Y. Xu, J. Wu, H. Zhang, L. Yang, D. X. Lun, Y. C. Hu, and B. Liu, "Picrosirius-Polarization Method for Collagen Fiber Detection in Tendons: A Mini-Review," Orthop Surg, vol. 13, no. 3, pp. 701-707, May 2021, doi: 10.1111/os.12627.

[54] D. Alves, M. A. Cerqueira, L. M. Pastrana, and S. Sillankorva, "Entrapment of a phage cocktail and cinnamaldehyde on sodium alginate emulsion-based films to fight food contamination by Escherichia coli and Salmonella Enteritidis," Food Research International, vol. 128, p. 108791, 2020/02/01/ 2020, doi: https://doi.org/10.1016/j.foodres.2019.108791.

[55] S. R. Derkach, N. G. Voron'ko, N. I. Sokolan, D. S. Kolotova, and Y. A. Kuchina, "Interactions between gelatin and sodium alginate: UV and FTIR studies," Journal of Dispersion Science and Technology, vol. 41, no. 5, pp. 690-698, 2020/04/15 2020, doi: 10.1080/01932691.2019.1611437.

[56] B. Iqbal, N. Muhammad, A. Jamal, P. Ahmad, Z. U. H. Khan, A. Rahim. A. S. Khan, G. Gonfa, J. Iqbal, and I. U. Rehman, "An application of ionic liquid for preparation of homogeneous collagen and alginate hydrogels for skin dressing," Journal of Molecular Liquids, vol. 243, pp. 720-725, 2017/10/01/ 2017, doi: https://doi.org/10.1016/j.molliq.2017.08.101.

[57] S. Shin, M. Ikram, F. Subhan, H. Y. Kang, Y. Lim, R. Lee, S. Jin, Y. H. Jeong, J.-Y. Kwak, Y.-J. Na, and S. Yoon, "Alginate–marine collagen–agarose composite hydrogels as matrices for biomimetic 3D cell spheroid formation," RSC Advances, 10.1039/C6RA01937D vol. 6, no. 52, pp. 46952-46965, 2016, doi: 10.1039/C6RA01937D.

[58] P. Sobhanian, M. Khorram, S.-S. Hashemi, and A. Mohammadi, "Development of nanofibrous collagen-grafted poly (vinyl alcohol)/gelatin/alginate scaffolds as potential skin substitute," International Journal of Biological Macromolecules, vol. 130, pp. 977-987, 2019/06/01/ 2019, doi: https://doi.org/10.1016/j.ijbiomac.2019.03.045.

[59] Z. S. Silva Junior, S. B. Botta, P. A. Ana, C. M. Franca, K. P. Fernandes, R. A. Mesquita-Ferrari, A. Deana, A. and S. K. Bussadori, "Effect of papain-based gel on type I collagen--spectroscopy applied for microstructural analysis," Sci Rep, vol. 5, p. 11448, Jun 23 2015, doi: 10.1038/srep11448.

[60] J. H. Kim, A. J. Kolozsvary, K. A. Jenrow, and S. L. Brown, "Mechanisms of radiation-induced skin injury and implications for future clinical trials," (in eng), Int J Radiat Biol, vol. 89, no. 5, pp. 311-8, May 2013, doi: 10.3109/09553002.2013.765055.

[61] R. Xu, H. Xia, W. He, Z. Li, J. Zhao, B. Liu, Y. Wang, Q. Lei, Y. Kong, Y. Bai, Z. Yao, R. Yan, H. Li, R. Zhan, S. Yang, G. Luo, and J. Wu, "Controlled water vapor transmission rate promotes wound-healing via wound re-epithelialization and contraction enhancement," Scientific Reports, vol. 6, no. 1, p. 24596, 2016/04/18 2016, doi: 10.1038/srep24596.

[62] S. Khodabakhsh Aghdam, A. B. Khoshfetrat, R. Rahbarghazi, H. Jafarizadeh-Malmiri, and M. Khaksar, "Collagen modulates functional activity of hepatic cells inside alginate-galactosylated chitosan hydrogel microcapsules," (in eng), Int J Biol Macromol, vol. 156, pp. 1270-1278, Aug 1 2020, doi: 10.1016/j.ijbiomac.2019.11.164.

[63] J. Zhou, K. Zhang, S. Ma, T. Liu, M. Yao, J. Li, X. Wang, and F. Guan, "Preparing an injectable hydrogel with sodium alginate and Type I collagen to create better MSCs growth microenvironment," e-Polymers, vol. 19, no. 1, pp. 87-91, 2019, doi: doi:10.1515/epoly-2019-0011.

[64] Y. Jalilpour, B. Abdollahzadeh, G. Parvizifard, M. Aghazadeh, A. Zahedi bialvaei, and H. Kafil, "The simple route for preparation of pH-sensitive hydrogels by using egg white proteins in Alginate scaffold for the encapsulation of probiotics," Ars Pharmaceutica, vol. 58, pp. 127-136, 11/01 2017, doi: 10.4321/S2340-98942017000300006.

[65] S. Popov, N. Paderin, D. Khramova, E. Kvashninova, O. Patova, and F. Vityazev, "Swelling, Protein Adsorption, and Biocompatibility In Vitro of Gel Beads Prepared from Pectin of Hogweed Heracleum sosnówskyi Manden in Comparison with Gel Beads from Apple Pectin," (in eng), Int J Mol Sci, vol. 23, no. 6, Mar 21 2022, doi: 10.3390/ijms23063388.

[66] S. R. U. Rehman, R. Augustine, A. A. Zahid, R. Ahmed, M. Tariq, and A. Hasan, "Reduced Graphene Oxide Incorporated GelMA Hydrogel Promotes Angiogenesis For Wound Healing Applications," (in eng), Int J Nanomedicine, vol. 14, pp. 9603-9617, 2019, doi: 10.2147/IJN.S218120.

[67] C. Vidal, P. Alves, M. M. Alves, M. J. Carmezim, M. H. Fernandes, L. Grenho, P. Inacio, F. B. Ferreira, T. G. Santos, and C. Santos, "Fabrication of a biodegradable and cytocompatible magnesium/ nanohydroxyapatite/fluorapatite composite by upward friction stir processing for biomedical applications," Journal of the Mechanical Behavior of Biomedical Materials, vol. 129, 2022.

[68] C. M. Tierney, M. G. Haugh, J. Liedl, F. Mulcahy, B. Hayes, and F. J. O'Brien, "The effects of collagen concentration and crosslink density on the biological, structural and mechanical properties of collagen-GAG scaffolds for bone tissue engineering," J Mech Behav Biomed Mater, vol. 2, no. 2, pp. 202-9, Apr 2009, doi: 10.1016/j.jmbbm.2008.08.007.

[69] L. E. Feinendegen, M. Pollycove, and C. A. Sondhaus, "Responses to low doses of ionizing radiation in biological systems," (in eng), Nonlinearity Biol Toxicol Med, vol. 2, no. 3, pp. 143-171, 2004, doi: 10.1080/15401420490507431.

[70] M. Li, L. You, J. Xue, and Y. Lu, "Ionizing Radiation-Induced Cellular Senescence in Normal, Non-transformed Cells and the Involved DNA Damage Response: A Mini Review," (in eng), Front Pharmacol, vol. 9, p. 522, 2018, doi: 10.3389/fphar.2018.00522.

[71] M. M. Acharya et al., "Consequences of ionizing radiation-induced damage in human neural stem cells," (in eng), Free Radic Biol Med, vol. 49, no. 12, pp. 1846-55, Dec 15 2010, doi: 10.1016/j.freeradbiomed.2010.08.021.

[72] B. V. Slaughter, S. S. Khurshid, O. Z. Fisher, A. Khademhosseini, and N. A. Peppas, "Hydrogels in regenerative medicine," (in eng), Adv Mater, vol. 21, no. 32-33, pp. 3307-29, Sep 4 2009, doi: 10.1002/adma.200802106.

[73] J. A. R. Barros, L. D. R. Melo, R. Silva, M. P. Ferraz, J. Azeredo, V. M. C. Pinheiro, B. J. A. Colaco, M. H. R. Fernandes, P. S. Gomes, and F. J. Monteiro, "Encapsulated bacteriophages in alginate-nanohydroxyapatite hydrogel as a novel delivery system to prevent orthopedic implant-associated infections," Nanomedicine-Uk, vol. 24, p. 102145, Feb 2020, doi: 10.1016/j.nano.2019.102145.

[74] B. Hissa, B. Pontes, P. M. Roma, A. P. Alves, C. D. Rocha, T. M. Valverde, P. H. Aguiar, F. P. Almeida, A. J. Guimarães, C. Guatimosim, A. M. Silva, M. C. Fernandes, N. W. Andrews, N. B. Viana, O. N. Mesquita, U. Agero, and L. O. Andrade, "Membrane cholesterol removal changes mechanical properties of cells and induces secretion of a specific pool of lysosomes," (in eng), PLoS One, vol. 8, no. 12, p. e82988, 2013, doi: 10.1371/journal.pone.0082988.

[75] M. Kaushik, R. Niranjan, R. Thangam, B. Madhan, V. Pandiyarasan, C. Ramachandran, D.-H. Oh, and G. D. Venkatasubbu, "Investigations on the antimicrobial activity and wound healing potential of ZnO nanoparticles," Applied Surface Science, vol. 479, pp. 1169-1177, 2019/06/15/ 2019, doi: https://doi.org/10.1016/j.apsusc.2019.02.189.

Supplementary Material

A. ATR-FTIR spectra of freeze-dried Alg and Alg-Coll samples incubated at 37 ºC for 12 h.